On the origin of Arctic Plastic

Interconnectivity between the Pacific and Atlantic Ocean and implications for plastic accumulation and transport in the Arctic

Anneke Louise Vries

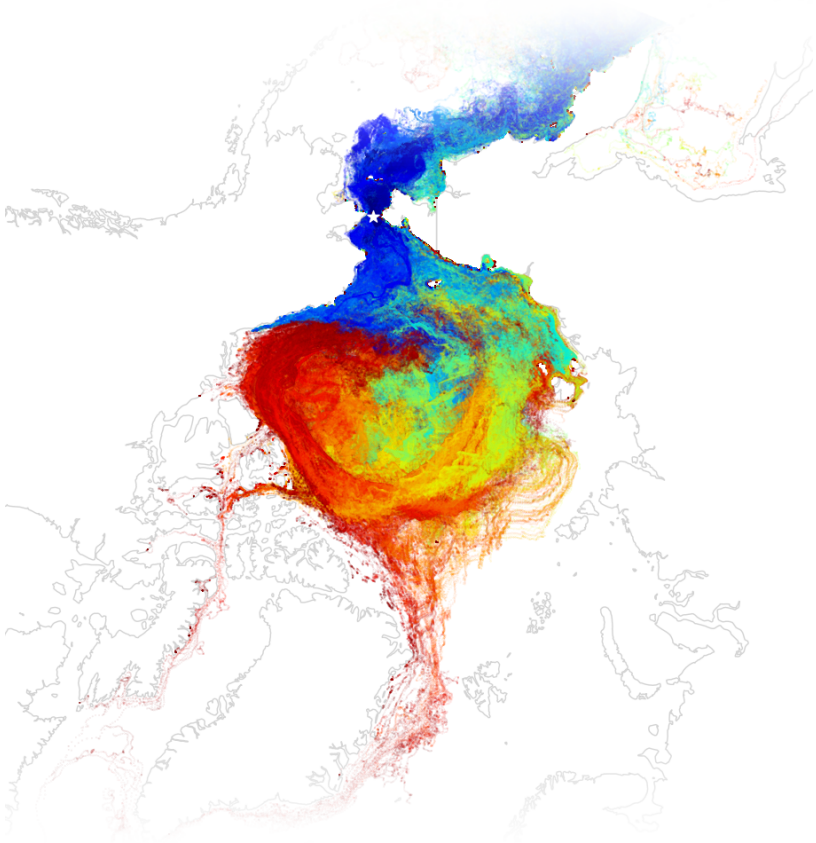

Master Thesis
Climate Physics

Supervisors
Dr. Erik van Sebille
Mikael Kaandorp
July 2019

Utrecht University

IMAU
Institute for Marine and Atmospheric research Utrecht

Abstract

Plastic pollution in the ocean is a growing concern. Yet, less than 1% of the total load of plastic going into the ocean is located, hence the quest for the lost plastic is still ongoing. Currently, microplastics are even found in remote areas such as the Arctic. Not only is plastic found floating in surface waters, but also in increased concentrations in sea ice. Even though many global modelling studies on plastic in the ocean have been performed, mechanisms for transport of plastic in the Arctic sea ice specifically, and entrainment of microplastic in ice, have not been studied yet by numerical modelling. The Arctic is especially interesting because it is changing rapidly under global warming. This thesis aims to study transport mechanisms of plastic and interconnectivity between the Atlantic, Arctic and Pacific Ocean using Lagrangian techniques and identifying accumulation zones in sea ice and the ocean. Floating particles that enter the Arctic Ocean from the Pacific side accumulate in the Beaufort Gyre and very rarely (0.3% of the particles) cross the Arctic to the Atlantic side when traveling in sea ice. Floating particles from the Atlantic Side either accumulated in the Barents Sea or are advected back to the Atlantic by the Transpolar Drift Stream, but do not enter the high Arctic. These results indicate the necessity of a realistic data set to simulate plastic transport and a parametrization for the entrainment of plastic in ice, and more research on accumulation of plastic in ice.

Contents

1 Introduction

Plastic pollution is a growing concern. Mismanaged plastic waste can enter the ocean and it was estimated that 4.8 to 12.7 million tonnes entered the ocean in 2010 alone, and without improvements in waste management this number is expected to have grown an order of magnitude by 2025 (Jambeck et al., 2015). Plastic items that enter the ocean can break down into smaller pieces called microplastics. Microplastics have the potential to harm the environment and human health by entering the (marine) food chain, act as a carrier for diseases and invasive species, or adsorb toxic (waterborne) contaminants (Cole et al., 2011; Barnes et al., 2009; Wright and Kelly, 2017; Viršek et al., 2017). For these reasons, more and more studies have been published on microplastics (figure 1.1).

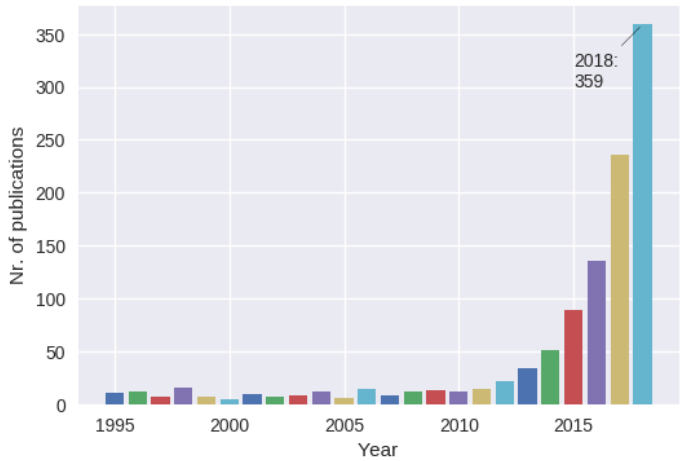

Figure 1.1: Number of publications per year on microplastic, based on Web of Science statistics. The search term was 'microplastic'.

Different studies have used different definitions for microplastics, but Frias and Nash (2018) defined microplastics as plastic particles with a size between 1 µm and 5 µm. Microplastics can be divided into two categories. Primary microplastics are plastics that enter the ocean as tiny particles, e.g. microplastics in scrubbing cosmetics or fibres from clothing. The second category is secondary microplastic: plastic that enters the ocean as big piece (e.g. a plastic bottle), and is broken down

due to biological, chemical and physical processes in the ocean (Cole et al., 2011). Most measurements of microplastics are taken in the North Atlantic and North Pacific, and other locations are sampled less intensively (Van Sebille et al., 2015). But with help of a model, it was estimated that the amount of plastic accumulated in the surface ocean was between 93 and 236 thousand tonnes in 2014 (Van Sebille et al., 2015). Even though this is a large number, this is only about 1% of the amount Jambeck et al. (2015) estimated for plastic entering the ocean in 2010 alone. Therefore, it is important to find the remaining amount of plastic.

The plastic entering the ocean accumulates in the middle of the subtropical gyres, in regions called the "Garbage Patches" (Van Sebille et al., 2012). The anticyclonic currents cause convergence in the middle of the gyre due to Ekman transport (Onink et al., 2019). The convergence of water causes downwelling in these regions and since most plastic floats, it stays at the surface. Recently, the possibility of a sixth garbage patch in the Arctic was identified in both models and observations (Peeken et al., 2018b; Bergmann et al., 2017; Kanhai et al., 2018; Mu et al., 2019), specifically in the Barents Sea (Cózar et al., 2017; Van Sebille et al., 2012). The Barents Sea is a potential hotspot for accumulation of microplastic, because there is downward movement (as is the case in the centre of the subtropical gyre) the Barents Sea is a sea where warmer denser water from the Atlantic is forced down due to the interaction with fresher and colder water. It is suspected that the source of the plastic in this potential accumulation zone is the Atlantic, because population density in the coastal areas in the Arctic is low, and therefore plastic waste contribution from the coastal Arctic is low (Cózar et al., 2017). Apart from the Barents Sea, observations point at relatively high plastic concentrations in sub-surface water between Greenland and Svalbard (up to 31.5 particles per liter (N/L)), and a lower concentration in the central Arctic Ocean sub-surface water (Kanhai et al., 2018). However, Peeken et al. (2018a) point out that microplastic concentrations (in N/L) found in (sub)surface water are orders of magnitude lower than concentrations in sea ice and in the deep sea. For example, the HAUSGARTEN observatory between Svalbard and Greenland showed concentrations of 42–6595 particles per kg (N/kg) in the deep sea sediments (Bergmann et al., 2017). Since the highest concentrations were found at the southernmost station, a possible explanation would be that plastic entrained in sea ice was transported with the Transpolar Drift Stream and then released after sea ice came into contact with the warmer Atlantic waters and ice melted (Bergmann et al., 2017). In addition to the high concentrations in the deep sea floor, high concentrations of microplastics are observed in Arctic sea ice (frozen sea water). Plastic found in sea ice cores had concentrations up to 4500 particles per liter (N/L) (Peeken et al., 2018b; Obbard et al., 2014). Furthermore, sea ice

has the potential of functioning as a long range transport mechanism (Obbard, 2018; Peeken et al., 2018b), and it is known that suspended matter accumulates in sea ice (Smedsrud, 2001, 2002). In addition, sea ice cover has the potential to influence microplastic concentrations by preventing mixing from wind, blocking influx of polluted waters and as a temporary source or sink (Kanhai et al., 2018). The exact role of sea ice in any of these mechanisms for storing or transporting microplastic is not well understood yet and this leaves room for further investigation. Peeken et al. (2018b) touched upon the modelling aspects of plastic in sea ice, by backward tracking sea ice cores to its possible origin. However they left out transitions between sea ice and ocean and diffusivity of sea ice. Hence, no extensive modelling studies for plastic in sea ice have been performed so far, unlike its counterpart for modelling plastic in the ocean (Van Sebille et al., 2012; Onink et al., 2019).

The processes governing plastic concentration, accumulation and transport in the Arctic are not well understood yet in today's climate, and the Arctic is changing dramatically: the sea ice volume, thickness and area are decreasing (figure A.10) (Simmonds, 2015). In order to take into account these changes in the physical environment and make estimates of future changes in plastic concentration, first the conditions nowadays need to be understood. Therefore this study aims to investigate the interconnectivity of plastic fluxes between the Pacific and the Atlantic Ocean and their contribution to plastic accumulation and transport in Arctic sea ice or in the ocean. I model the particle flow in the Arctic as a proxy for microplastic, with particle advection either by sea ice or by ocean currents. First of all, I perform a validation of the method by comparing model results with buoy trajectories. In order to understand where microplastics come from and where they go, I study trajectories of particles flowing in ocean or with ice through the main Arctic entrances. Then, in order to elaborate on where plastic ends up, I identify accumulation patterns in the Arctic by using Markov Chains. Within these questions I also try to identify the role of sea ice. Chapter 2 gives the physical background of the region and theory behind the methods used. Chapter 3 discusses the methods and chapter 4 shows the results. Finally, chapter 5 interprets these results, puts them in a wider context and concludes the thesis.

2 Theory

In this chapter, I discuss the theory that is the basis for the analysis in this thesis, because it gives an insight on why certain choices are made and helps in the interpretation. First of all, I give an introduction to the Arctic Ocean and important dynamic features, followed by a discussion of important mechanisms for the formation, governing equations and other characteristics of sea ice. Then, I discuss Lagrangian modelling and finally, I discuss some of the concepts behind Markov Chains.

2.1 Arctic Ocean

The Arctic Ocean is different from other oceans due to the fact that is almost entirely enclosed by land, that a large part is covered by sea ice, and due to its location in the high latitudes (figure 2.1). In the Arctic Ocean typical scales for the Rossby radius of deformation are between 5 and 15 km, which is much lower than other places on the planet and it influences how well mesoscale features are modelled (Nurser and Bacon, 2014). The first baroclinic Rossby radius of deformation is associated with a 'typical' scale of oceanic features such as boundary currents and eddies. Eddies are important because they promote mixing in the ocean and cause divergence of pathways.

The second thing that makes the Arctic extraordinary is that its basin is almost entirely enclosed by land, and therefore there are only a few connections with other oceans. On the Pacific side there is a connection with the Bering Strait. The Bering Strait is very shallow ($\sim$50 m) and narrow ($\sim$85 km), but the connection is still important because of its low salinity water inflow, which is mostly northward (Rudels, 2015). The inflow varies over the decades, but also seasonally. For example, a small cyclonic boundary current develops in summer flowing from the Bering Strait along the Canadian coast (figure A.1), as opposed to the mean anticyclonic Beaufort Gyre movement. Estimates for the volume flowing in are around 1 Sverdrup (Sv) (Rudels, 2015; Tsubouchi et al., 2018). On the Atlantic side more water flows along the coast of Norway into the Arctic, about 2-8 Sv (Weeks and Hibler, 2010). The Norwegian Current splits into the West Spitsbergen Current (WSC)

and North Cape Current that flows into the Barents Sea (figure A.2). The relatively warm and salty water originating from the Gulf Stream enters the Barents Sea, hence it is very often ice free there. Furthermore, density of the water flowing in from the Atlantic is different from in the Arctic (relatively warm, saline and dense), hence Atlantic water is pushed under the colder and fresher water in the Barents Sea: there is a front in the water and little diapycnal mixing is happening (Rudels, 2015). In other words, there are mechanisms for downward transport here, and a clear division between different water masses (Cózar et al., 2017; Weeks and Hibler, 2010). The difference in water masses is also important on the Pacific side, where relatively fresh water enters the Arctic Ocean via the Bering Strait. A schematic representation of the different water masses can be found in figure A.3.

There are just a few places where water and ice leaves the Arctic. The main current flowing out of the Arctic is the East Greenland Current (E GC). It flows south in the Fram Strait (figure A.4) and is estimated to be 3-5 Sv (Weeks and Hibler, 2010). Those values are of the same order of magnitude found by Tsubouchi et al. (2018) in table 2.1. The East Greenland Current is also the main export mechanism of sea ice out of Arctic, carrying 4000-5000 m^3 ice south each year (Weeks and Hibler, 2010). Other, smaller pathways for both sea ice and water out of the Arctic are either through the Canadian Arctic Archipelago (CAA) or the Nares and Davis Strait (table 2.1). Another pathway for sea ice out of the Arctic is south through the Bering Strait, pushed by northerly winds in winter. In the Arctic Basin itself, there are two main sea ice drift features (figure A.5). The first feature is the Transpolar Drift Stream (TDS) that flows from north of Nova Zembla to the Atlantic Ocean, ending in the East Greenland Current. The other feature is the Beaufort Gyre, an anticyclonic circulation both visible in ice and in the surface ocean.

Thirdly, a unique feature of the Arctic is that it is covered by seasonally varying sea ice. Sea ice area and volume have been diminishing over the past 35 years (Simmonds, 2015), accompanied by a thinning of sea ice in the Fram Strait and a decrease of average ice age from 3 to 2 years in the period 1990-2012 (Krumpen et al., 2016). Ice thickness is relevant for particle entrainment, because the temporary sink or transport mechanism is more relevant if the plastic stays in ice longer. Multiyear ice has survived one or more summers and is typically thicker than first year ice. In addition, thicker ice is sometimes a sign of (wind-driven) convergence. South of the Beaufort Sea, west of Canadian archipelago and north of Greenland are known regions where older and thicker ice survives the summer (Kwok and Cunningham, 2010; Kwok, 2015) (figure A.6).

The Beaufort Gyre is important in this thesis for the interpretation of accumulation zones, hence

Table 2.1: Volume transport in and out the Arctic for ocean currents and sea ice. Net monthly mean over the period September 2005-August 2006. Positive is into the Arctic. Barents Sea Opening is located just after the WSC splits off the North Cape Current. Davis Strait is west of Greenland, south of the Nares Strait. After Tsubouchi et al. (2018)

	Ocean volume transport (Sv)	**Sea ice volume transport (mSv)**
Davis	-2.1 ± 0.7	-9 ± 10
Fram (EGC + WSC)	-1.1 ± 1.2	-51 ± 34
Barents Sea Opening	2.3 ± 1.2	—
Bering	0.7 ± 0.7	∼ 0

it is discussed a bit more in detail here. The Beaufort Gyre has been a subject of recent studies and varies in strength and shape (Regan et al., 2019; Proshutinsky and Krishfield, 2019). The Beaufort High (atmospheric pressure) forces the Beaufort Gyre and therefore also determines its strength (Regan et al., 2019; Proshutinsky et al., 2009). In general, wind over the ocean causes a net transport (in the ocean boundary layer) at a ninety degree angle to the wind. In the Arctic, the transport is to the right of the wind direction and thus relatively fresh and cold water is transported from the edges to the center and builds up here (Proshutinsky et al., 2009). The layer of colder water isolates sea ice from the warmer water below (Doddridge et al., 2019). It is interesting to study freshwater accumulation, since like plastic, freshwater floats on heavier saltier water, which is the water mass underneath. The freshwater is not purely without salt, but usually the fresh water content of a water mass is calculated and separated in models as if it were a separate water mass. In reality, mixing is going on, but the fresh water 'bubble' is a good analogy (Proshutinsky et al., 2009). Still, the 'bubble' has a certain depth, which is not like the assumption made for plastic: floating at the surface. However, microplastics are transported by the water (and ice) and therefore the mechanisms forcing the flow still affects the microplastic distribution.

The accumulation of fresh water in the middle of the gyre is governed by a balance of mechanisms (Doddridge et al., 2019). The three mechanisms to keep the gyre in equilibrium are wind stress on the ice free part of the Beaufort Gyre, eddies that tend to flatten the halocline, and the Ice-Ocean governor: the difference between ice and ocean velocity and hence the transfer of momentum from one medium to the other. To elaborate on this, wind stress due to the Beaufort High on the open ocean causes convergence and so does the transfer of momentum from ice to the ocean, as the ice is forced by the same wind pattern. However, the fresh water bubble has a finite depth in the models and therefore there must be a mechanism that counteracts this convergence. The 'bubble' causes a steepening of the halocline and as a response to the difference in density between centre and edge of the gyre, eddies tend to mix water masses to flatten the halocline and hence to counteract

convergence. These three mechanisms together keep the Beaufort Gyre in equilibrium (Doddridge et al., 2019), which is important in explaining accumulation zones later in this thesis.

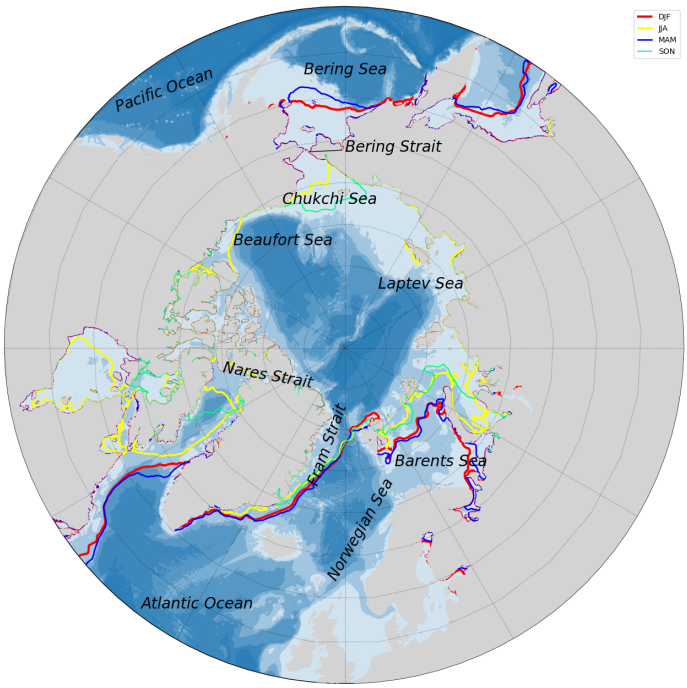

Figure 2.1: Map of domain used in this thesis. Different contours show sea ice extent average over the different seasons in the period 2014-2016. The domain is 50°N-90°N.

The physical environment of the Arctic has been changing over the past decades. Also the main drift patterns I described previously have undergone some changes. Both the Beaufort Gyre and the Transpolar Drift Stream strengthened over the past 28 years (Kwok et al., 2013). Not only did the Beaufort Gyre strengthen, it also expanded in the period 2003-2014 (Regan et al., 2019). The gyre size also changes with the season: its area halves in summer. Regan et al. (2019) emphasize that the strength of the gyre depends, among other factors, on its location. The bathymetry varies in the Arctic Basin and thus in the region of the Beaufort Gyre. More specifically, the Chukchi Sea (south west of the Beaufort Sea) is much shallower than the Beaufort Sea (figure 2.1), and this influences the symmetry of the Beaufort Gyre. Many currents in the Arctic follow contours of equal f/H and if the water depth (H) changes, this influences the current because it is not in the same equilibrium as before (f is the Coriolis parameter). A possible expression of the change in gyre size can be the shift in freshwater inflow into the Beaufort Gyre: Kelly et al. (2019) found that the Lagrangian trajectories into the Beaufort Gyre changed over the decades, from a convergence zone ('a waiting room') in the Chukchi Sea in the 1980s to a direct pathway into the Beaufort Gyre in the 1990s and early 2000s. This shift in trajectories is a further manifestation of the asymmetry and might be related to the increased strength and area of the Beaufort Gyre (Regan et al., 2019).

Therefore, variation in the Beaufort gyre might be important for explaining interannual variation of plastic distribution.

2.2 Sea ice physics

In order to understand how plastic is transported by sea ice and in the Arctic in general, it is important to understand how it enters sea ice and therefore also how it is modelled, both for the data used, which is based on a coupled sea ice-ocean model, and to parametrize and understand transitions between ocean and sea ice, in order to model Lagrangian trajectories of particles. Therefore this section first introduces mechanisms of sea ice thickness variations and consequently particle entrainment. Next are sections on how this is parametrized in models, both thermodynamically and dynamically.

Different processes increase or decrease the thickness of ice: on the one hand dynamic processes change ice thickness (convergence or divergence). Divergent stresses pull sea ice apart leading to thinning of the ice, and even though it is less common, sea ice also converges under high wind stresses, e.g. in the Laptev Sea and North of Greenland (Kwok, 2015). Either pressure ridges are created, or sea ice floes (floating pieces of sea ice) raft on top of each other. On the other hand, thermodynamic processes in- or decrease of sea ice thickness, i.e. water freezes to already existing ice pack or melts away. Since sea ice works as an insulator from the cold atmosphere, complicated processes for freezing dominate (Weeks and Hibler, 2010), even though these processes are usually neglected when modelling (as in equation (2.2)). An example of a complicated process is the following: sea ice thickness can also increase when sea water flushes over the already existing sea ice pack and then freezes or precipitated snow compacts and changes into ice. Often combinations of thermodynamic and dynamic processes occur.

Particle entrainment

Particle entrainment happens if suspended particles are included in sea ice. So far, no research has been performed regarding entrainment of plastic particles in sea ice. However, other types of particles captured in sea ice have been studied in the past. The first to introduce sea ice as a potential mechanism for long term transport of contaminants was Pfirman et al. (1995), who identified distribution of heavy metals and organochlorines. However, a few years before Reimnitz et al. (1993) already described possible mechanisms for entrainment of particles, such as sediments and algae. The mechanism works as follows: frazil ice forms in super cooled water (e.g. caused by wind blowing over the water with very low temperatures) and scavenges particles, i.e. small ice 'disks' or 'needles' form underwater and consequently capture particles when floating to the surface (figure 2.2). At the surface, frazil ice freezes to the existing pack and therefore includes particles in

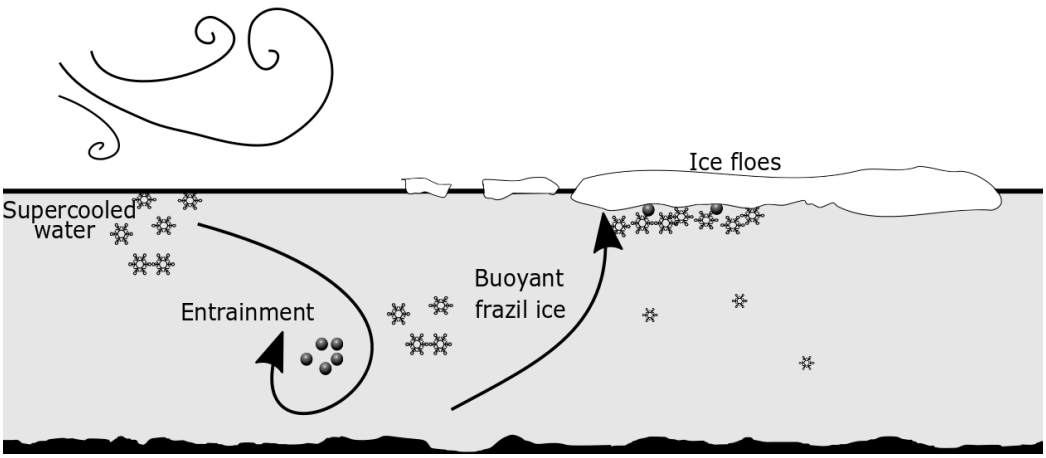

Figure 2.2: Simple schematic reprensentation of frazil ice entraining particles. Based on figure 1 of Daly (2008)

the ice layer. This mechanism is so efficient that particle concentrations in ice can be much higher than the water underneath. Other mechanisms of enrichment of particles in ice are nucleation (new ice forms on foreign particles) or mixing of surface-formed flocks through turbulence and thereby capturing particles before joining the ice layer (Reimnitz et al., 1993). In this thesis I am interested in how particles that were suspended in water are entrained and transported by ice, therefore I assume that sea ice grows mostly from the bottom and is efficient in capturing particles.

Sea ice was found to be efficient in trapping mater. Darby et al. (2011) found layers of sediment in sea ice, with concentrations up to $7\,\mathrm{kg/m^2}$ and layers of up to 10 cm. The proposed mechanism was anchor ice formation: Part of the sea floor freezes and when buoyant enough rises and is included in sea ice. However, the mechanism of suspension freezing (scavenging by Reimnitz et al. (1993)), usually dominates (Darby et al., 2011). Entrained particles have a maximum size from 12-211 µm, but above 30-60 µm it is likely due to anchor ice, because these particles are larger and less likely to be captured through scavenging (Darby et al., 2011). About a quarter to a third of the sediment in ice floes is from different origins: ice mixes after freezing, for example due to rafting or pressure ridges. Apart from field observations, experiments were done. Smedsrud (2002, 2001) aimed to investigate the efficiency of capturing suspended sediment into sea ice due to frazil ice scavenging. In a wave tank, sediment entrainment factors (equation (2.1)) had values of 2-4 after 24 hours with a maximum of 10 times more sediment in ice than in the water underneath. A model was able to reproduce this result (Smedsrud, 2002). I suspect that a similar accumulation of particles in ice can be found in regions with leads (fractures in sea ice), or other open water next to a sea ice edge, because these regions have the turbulence / mixing due to wind that is needed for this entrainment. Smedsrud (2002) also found that not only wind (influencing turbulence) but also low air temperatures

(influencing heat flux, hence freezing of frazil ice) are very important for high sediment entrainment factors. All in all, these studies suggest that there are mechanisms that promote accumulation of entrained plastic particles in sea ice.

$$SEF = \frac{\text{concentration matter in ice}}{\text{concentration suspended matter in water}} \tag{2.1}$$

Thermodynamic equations

Plastic entrainment into ice has so far not been studied in an experimental study, but also not in a model study. Therefore it is important to understand how sea ice is modelled in the data used for Lagrangian particle tracking and the limitations of these models. The thermodynamic part of sea ice is usually described as follows.

The different mechanisms of freezing ice are usually parametrized in models. A simple model of a sea ice slab through heat fluxes was developed by Maykut (1978) and described in Weeks and Hibler (2010) and schematically represented in figure 2.3, with a layer of water, a layer of ice and air above. In this figure, H is ice thickness, ρ_i ice density, T_f freezing point (assumed at ice water interface), T_a is air temperature, and T_o ice surface temperature (controlled by heat balance, not necessarily equal to T_a) and F the heat flux. If F_w is positive (heat coming in from water) ice melts, and when negative, ice growths. The amount of growth at the bottom is determined by the sum of F_c and F_w. It is assumed that there is no water on top of the ice layer, hence it can not grow from the top. In reality there is some snow, and water flushing over the sea ice, but this is not considered in this model. When assuming : $F_w \approx 0$, $F_t = C_t(T_a - T_o)$ (rate of heat exchange ice atmosphere dependent on difference T_a and T_o with averaged surface heat transfer coefficient C_t) and adding snow cover this results in the following:

$$H^2 + [\frac{2k_i}{k_s}H_s + \frac{2k_i}{C_t}]H = \frac{2k_i}{\rho_i L}\theta \tag{2.2}$$

where θ is the cumulative number of freezing degree days, and k_i, k_s, L and H_s are the thermal conductivity for ice, thermal conductivity for snow, latent heat for vaporization and snow thickness, respectively (Weeks and Hibler, 2010). The snow cover does not contribute to the formation of ice

in this model, only as an extra insulation layer. Or

$$H^2 + (13.1H_s + 16.8)H = 12.9\theta$$

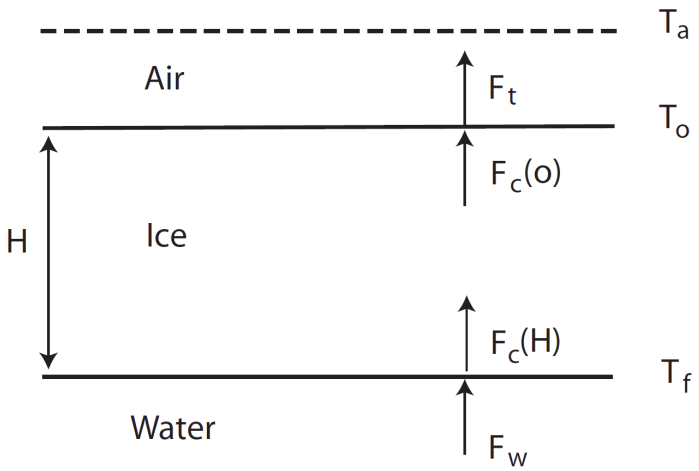

Figure 2.3: Figure 4.4 from Weeks and Hibler (2010). *Schematic of a slab of snow-free sea ice showing the pertinent heat fluxes.*

Dynamic equations

One of the first efforts describing sea ice movement was a formula (2.3) introduced by Hibler III (1979), and is still very often used in models such as NEMO-LIM2 (Vancoppenolle et al., 2009), and hence important for this thesis as assimilated data with the NEMO-LIM2 model was used. As opposed to the thermodynamic equation (2.2), equation (2.3) is the momentum balance. Therefore, equation (2.3) can be interpreted as the dynamics of the sea ice and hence it gives insight into the forces determining the movement.

$$\frac{Dm\vec{u}}{Dt} = \vec{\tau_a} + \vec{\tau_w} - mf\vec{k} \times \vec{u} - mg\nabla H - \mathbf{F} \tag{2.3}$$

Equation (2.3) shows the ice momentum balance. It is influenced by atmospheric stresses ($\vec{\tau_a}$), oceanic stresses ($\vec{\tau_w}$), Coriolis force ($mf\vec{k} \times \vec{u}$), gravitational forces caused by height differences ($mg\nabla H$) and internal stress variation. The wind also forces the ocean, but also has a direct effect on sea ice and usually is the biggest driver of sea ice movement (Spreen et al., 2011) and also visible from figure A.7. Different mechanisms have been proposed for determining the elasticity and the viscosity of the ice, and also newer versions of the LIM-model have been developed, but this

is not integrated yet in the reanalysis data, probably due to the lack of accuracy in ice thickness (Vancoppenolle et al., 2009; Hunke and Dukowicz, 1997). The main drawback of modelling the sea ice (both thermodynamically and dynamically) is that processes governing sea ice thickness are usually more complex than in equations (2.2) and (2.3), e.g. rafting or pressure ridges. This leads to uncertainties in thickness.

2.3 Lagrangian modelling

Lagrangian modelling is a type of modelling often used in oceanography and atmospheric sciences and used in this thesis. For Lagrangian modelling, the trajectory of a virtual particle is calculated based on the velocities in a certain domain called a field. Usually the field not only contains velocities, but also other variables that can be sampled along a trajectory, e.g. temperature or sea ice thickness. The virtual particle can be a fluid parcel, but also another object that moves in a field. This other object can either be passive, e.g. a piece of plastic, or active with a response to environmental variables, e.g. an organism. In contrast, Eulerian modeling considers data at fixed locations, rather than along trajectories. Usually the effort of computing changes in the total (Eulerian) field is very large, hence it is often easier to analyze Lagrangian trajectories, even though the flow fields that need to be stored also take up much memory. In addition, Lagrangian modelling considers the variation of environmental variables along the trajectory history of a virtual particle, instead of locally, i.e. at one spot, which gives insight into the connectivity between different regions (Van Sebille et al., 2018). In my case, the trajectory history gives insight into e.g. how much time particles spent in sea ice on their way from the Pacific to the Atlantic Ocean.

Trajectories are modelled by the following equation (Lange and van Sebille, 2017):

$$\mathbf{X}(t+\Delta t) = \mathbf{X}(t) + \int_{t}^{t+\Delta t} \mathbf{v}(\mathbf{x},\tau)d\tau + \Delta\mathbf{X}_b(t) \tag{2.4}$$

The left hand side of equation (2.4) is the new position of the particle ($\mathbf{X}(t+\Delta t)$), and the right hand side contains the old position of the particle ($\mathbf{X}(t)$), the local velocity field ($\mathbf{v}$), and custom behaviour ($\mathbf{X}_b$) of the particle causing it to move more than it would as a passive particle. The custom particle behaviour is referred to as a kernel from now on.

2.4 Markov chains

One of the methods used to study movement of floating particles is the Markov Chain. Based on Lagrangian trajectories, it is possible to build a transition matrix. Transition matrices are used to describe the probability of tracer, or a fraction of particle trajectories, going from one cell to another cell in a gridded domain. For particles this means a fraction of many particles goes from one grid cell to a another grid cell, and the rest stays in the same grid cell. When a transition matrix is used to describe tracer, the "tracer density" has a certain probability to go to another grid cell and hence change the total density distribution. The Markov Chain method has been applied before in physical oceanography. Froyland et al. (2014) investigated the connectivity of global ocean surface through Markov Chains. They found five converging areas based on both density evolution (as in equation (2.5)) and eigenvectors (as in equation (2.8)), which they referred to as attractors. These attractors are centered in the gyres of the North and South Pacific and Atlantic Ocean and the Indian Ocean. The researchers also partitioned the ocean into basins of attraction based on backward evolution and the eigenvectors of the transposed matrix.

A transition matrix is constructed for a certain time interval (dt). In order to simulate the time evolution of the density distribution, the dot product of a transition matrix and the initial density distribution is taken (equation (2.5)). Using a transition matrix to simulate density over time is often computationally cheaper than calculating many individual trajectories over a long time period. However, one of the disadvantages is that information is lost because the distribution is only described by a more statistical approach instead of individual trajectories.

$$T \cdot \vec{v}_{t=0} = \vec{v}_{t=1dt} \tag{2.5}$$

In equation (2.5) T is the transition matrix, $\vec{v}_{t=0}$ the initial density distribution, and the distribution after one time step is $\vec{v}_{t=1dt}$.

Example

An example sketch is made in figure 2.4. Every grid cell has an index, in the example only 0 or 1. The column index is the index belonging to the grid cell where a particle starts and on the rows the index indicates where the particle ends up (see equation (2.6)). Then the matrix is column normalized (see equation (2.7)).

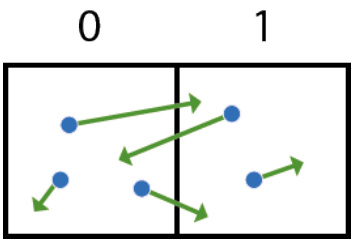

Figure 2.4: Sketch of how particles might move in a domain with two grid cells. The blue dots are the initial locations and the green arrows the displacement in $1 \times dt$

$$T = \begin{array}{c} \\ j{=}0 \\ j{=}1 \end{array} \begin{array}{c} \begin{array}{cc} i{=}0 & i{=}1 \end{array} \\ \begin{bmatrix} 1 & 1 \\ 2 & 1 \end{bmatrix} \end{array} \tag{2.6}$$

$$T = \begin{array}{c} \\ j{=}0 \\ j{=}1 \end{array} \begin{array}{c} \begin{array}{cc} i{=}0 & i{=}1 \end{array} \\ \begin{bmatrix} 0.33 & 0.5 \\ 0.66 & 0.5 \end{bmatrix} \end{array} \tag{2.7}$$

Stationary densities

Some systems contain an attractor. Attractors are regions in a domain where eventually all particles (or tracer) will end up after infinite time. This final equilibrium distribution after infinite time is also called the stationary distribution. Exchange between different grid cells can still take place but does not affect the overall density. If in a system the distribution stays dependent on time it does not have an attractor. An example system without a stationary density is cylindrical domain with a particle traveling in circles. In order to find the stationary distribution, one could use the Markov chain method. Using a uniform initial distribution, and iterating this distribution with equation (2.5) until the distribution does not change anymore ($t \to \infty$), will give a stationary distribution if this exists. However, a more elegant way is to use the eigenvector belonging to eigenvalue $\lambda = 1$. If a final distribution does not change, it is the same as multiplying this distribution with one everywhere. Hence, if the exchange between different grid cells (the transition matrix) does not change the total density distribution, the final equilibrium distribution is reached. The following equation sheds some light on this:

$$T \cdot \vec{v}_{eigen} = \vec{v}_{eigen} \tag{2.8}$$

In equation (2.8), $\vec{v}_{eigen}$ is the right eigenvector belonging to eigenvalue $\lambda = 1$. Equation (2.8) can be interpreted as follows: for a certain distribution ($\vec{v}_{eigen}$), it does not matter how often the dot product with the transition matrix (T) is taken, it is equal to multiplying a factor 1 with the eigenvector, i.e. the distribution stays the same. The eigenvector can show where attractors in the Arctic Basin are

For a square transition matrix of size M, there are M eigenvectors. However, only the eigenvalues belonging to eigenvalue 1 indicate a stationary distribution. Eigenvalues with values close to one are slowly decaying distributions (Stuart, 2014). These slowly decaying structures might give insight into transient structures. In a complex system such as the ocean with sea ice, they are likely to be important, since they do point out transient features that might act as a attractor for a certain time scale shorter than ∞. Furthermore, not all matrices have a eigenvector with eigenvalue 1, therefore these slowly decaying distributions are extra important to study. .

A major difference between the studies done before on attractors in the ocean (Froyland et al., 2014; van der Mheen et al., 2019), is that this thesis does not have a closed system: it investigates only part of the global ocean and inherently loses 'mass' over time . This means that the external sink is an attractor, but in the system I can still get slowly decaying distributions. Stuart (2014) also identified slowly decaying transient sets in her analysis of the global ocean.

There are advantages and drawbacks to this method. One of the drawbacks of applying Markov chains is that it can lead to numerical diffusion of tracer, e.g. if the resolution is too coarse, particles on two sides of a boundary can be attributed to the same grid cell and therefore cause 'leaking' (McAdam and van Sebille, 2018). An example is across land in Panama or across a boundary current. In order to minimize this leaking, a fine resolution and a long simulation length should be chosen. The advantage of Markov Chains is that I can study accumulation specifically in ice, by removing seasonal variability and iterating one season over and over.

Also Van Sebille et al. (2012) used Markov Chains with an initial tracer distribution based on coastal population. They defined a tracer accumulation factor (TAF): the factor by which the initial tracer value has increased (or decreased) after a certain time. Not only did they find the five before mentioned convergent regions ("garbage patches") but also a sixth region in the Barents Sea, which recently seemed to be at least partially confirmed (Cózar et al., 2017).

3 Methods

In order to answer the research question what the connection for plastic between the oceans through the Arctic Ocean is, the following sub-questions are identified. Firstly, how well do virtual trajectories reproduce real trajectories? Secondly, what are pathways for floating particles entering the Arctic? Next, what are accumulation zones for particles in the Arctic? And finally, what is the influence of sea ice? This chapter first discusses the data used and its limitations, consequently discusses methods used for drifter comparison, the release and analysis of individual trajectories and accumulation zones.

3.1 Data

In order to advect particles along a trajectory, a background ocean velocity field is required, and in my case also the sea ice velocity field with accompanying variables such as sea ice thickness and concentration. The data used was provided by the Copernicus Monitoring Service, and is based on a coupled sea ice and ocean model, forced by reanalysis atmosphere data, and assimilated with several variables. This data is convenient because it has a relatively high resolution and is internally consistent (between ice and ocean). It is also expected to be better assimilated with observations than a non-assimilated run.

The input for the velocity field was Global Ocean Physics Reanalysis data from the Copernicus Monitoring Service (CMEMS) (Nouel, 2012). The data used has a daily resolution from 2001-2016 on a $1/12^o$ lat-lon grid. This reanalysis data is based on assimilated model output. The sea ice and ocean models are LIM2 EVP and NEMO 3.1 respectively. Bouillon et al. (2009); Fichefet and Maqueda (1997) accompanied the LIM2 model, based on equations (including equation (2.3)) of Hunke and Dukowicz (1997). The effective resolution is 10 km and the data set is eddy permitting, but not always eddy resolving. NEMO uses an ORCA grid, which is tripolar, but the regridded data has been provided on a lat-lon grid. Hence, some of the variables need to be interpreted with caution. The resolution is 1/12 degree, but this does not mean that the variables were explicitly

calculated for every grid point, hence they might give a false sense of accuracy. Some variables in the GLORYS12V1 data set are jointly assimilated: sea level anomaly, satellite sea surface temperature, sea ice concentration, sea ice thickness, in situ temperature and salinity vertical profiles. Data assimilation means that observational data and numerical model output are combined to optimize data for the evolving system (Zhang and Moore, 2015). The reanalysis sea ice concentration is assimilated with the quarter degree reanalysis and OSISAF (a satellite sea ice product). The former is assimilated with CERSAT (another satellite sea ice product). The variables I used are sea ice concentration and thickness, meridional and zonal ocean and ice velocities.

Accuracy of the data

There is no consensus on the quality of the sea ice variables in the data (GLORYS12V1), but the main ocean currents are reproduced well, as described in the quality document (Drévillon et al., 2018). Even though sea ice concentration in generally well reproduced, sea ice concentration is in general lower for the reanalysis data in comparison to an independent observations data set. In summer there is excess ice melt and in winter there is a reduced ice extent spread (Drévillon et al., 2018). This accompanying quality document also states that due to the assimilation the sea ice data is reliable for thickness and concentration. Demgen (2012) found that Lagrangian trajectories based on OSISAF satellite sea ice velocities (used for data assimilation) are in good agreement with buoy trajectories. Uotila et al. (2019) considered (among others) GLORYS2v4, which is similar to the data set used here, but with a lower resolution, and found that in general the sea ice edge is in good agreement with observations for the quarter degree data set, which is no surprise since sea ice data is assimilated with observations, in contrast to e.g. snow cover.

However, some studies found that thickness was not well reproduced in reanalysis data. Bouillon et al. (2013) found that it in the Canadian Archipelago, the deformation rates are noisy, which leads to unreliable ice thickness in this region. Also Chevallier et al. (2017), the first to compare reanalysis products with each other and with observations in the Arctic, found that in general the reanalysis data produces thicker ice in the Beaufort Gyre and thinner ice around the North Pole (NP) and north of the Canadian Arctic Archipelago (CAA) compared to the observations. The specific data set used for this thesis is not mentioned in the paper, but these features were found among all reanalysis products (Chevallier et al., 2017). Furthermore, ice drift speeds are higher than expected. This product underestimates the ice thicknesses north of CAA and around the North Pole up by up to 1 m and overestimates the Beaufort Gyre ice thickness up to 2 m.

3.2 Parcels

The module ocean parcels for python uses velocity fields to advect virtual particles back or forward in time (Lange and van Sebille, 2017) with equation 2.4. It also allows for sampling of 'field variables' along the way, e.g. temperature, sea ice thickness or sea ice concentration. Furthermore, custom 'behaviour' for particles can be added to the passive movement of the particle due to velocity fields. The custom behaviour is referred to as kernel and shown as $\Delta\mathbf{X}_b(t)$ in equation (2.4). I used the Runge-Kutta4 method for interpolation of particles in the field. In this study, particles could either move with sea ice (sea ice velocity *usi* and *vsi* from CMEMS) or ocean currents (ocean velocity *uo* and *vo* from CMEMS). I tested multiple kernels for determining with which medium the particles move. For most cases, the following (simple) formula was applied:

$$P = \begin{cases} \arctan(x - 0.15), & \text{if } x > 0.01 \\ 0, & \text{otherwise} \end{cases} \tag{3.1}$$

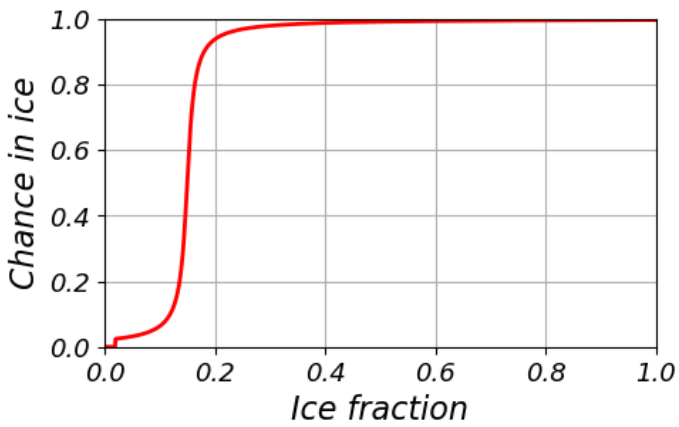

Figure 3.1: Schematic representation of equation (3.1). This kernel is referred to as the sea ice concentration (sic) kernel. The area under the the curve is the probability of a particle being in ice during every time step.

A random number was picked for every time step and if it was below the curve, the particle was assumed to be in ice. This means that usually, particles are considered to be in ice if the grid cell has an ice concentration higher than 15% and particles are forced to be in water for an ice concentration of 1% or less, also represented in figure 3.1. In literature 15% is a common percentage to represent the edge of the sea ice extent, and other percentages tested do not give the same values, but they do give the same trend (Parkinson et al., 1999; Fetterer et al., 2017; IPCC, 2013). In order to analyse the sensitivity of pathways to the definition of the sea ice edge, different percentages were used in

the sensitivity analysis (5, 30, 60 and 95 %). The parametrization of the transition is not based on explicit physical mechanisms, hence the 'randomness' introduces this uncertainty in the kernel, and furthermore it adds a certain diffusivity to the trajectories. Therefore this method is not more deterministic than what is known of reality. From now on this kernel will be referred to as the sea ice concentration (sic) kernel.

In addition, I tested a second, somewhat more complicated kernel. One of the drawbacks of equation (3.1) is, on top of the before mentioned somewhat arbitrary percentage, that it does not differentiate between the melt and growth season. Hence the following scheme is applied, as in figure 3.2:

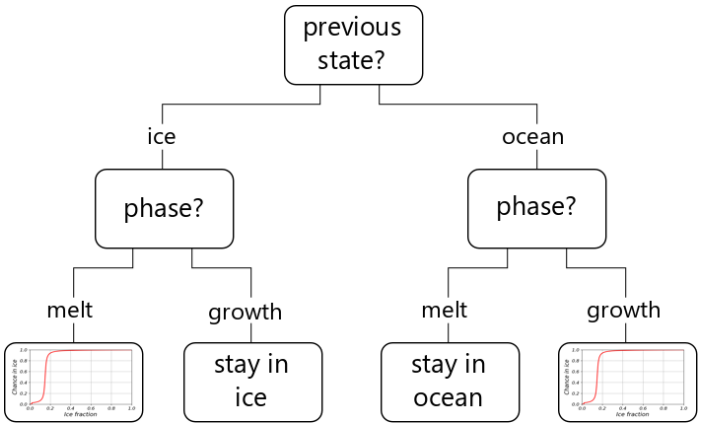

Figure 3.2: Schematic representation of second kernel applied. This kernel is referred to as the sea ice growth (sig) kernel. The final step is the equation (3.1) applied.

The idea behind this kernel (referred to as the sea ice growth (sig) kernel) is that the particles can only enter the sea ice in the growth season and leave the ice in the melt season. The phase depends on the change in sea ice thickness relative to the previous time step of the particle. Once the phase (melt or growth) is determined, formula (3.1) is applied by checking if a random number is lower than the function. Furthermore, one other advection kernel is used. In order to investigate the difference by only ocean and ocean+ice transport, a few simulations were done with only ocean advection. Depending on the goal of the simulation, a different kernel was used.

3.3 Drifter comparison

First of all, I discuss the difference between virtual particle trajectories and observed buoy trajectories. This gives insight in how accurate the other results are and it gives guidance in how to continue this research: whether to track individual cores or investigate the probability of particles going from one place to the next and focus on large groups of particles.

Drifter separation in literature

In order to quantify how good Lagrangian modelling performs relative to reality, many studies have been done. There are three approaches of comparing drifter data and modelled Lagrangian trajectories.

The first approach is intuitively simple: measuring the displacement and angle between the drifter and model trajectory. Bedi et al. (2019) used this method to evaluate drifter data to validate ocean models, including NEMO CMEMS in the low and midlatitudes. They found a mean daily displacement of 17 km for the CMEMS data. Also Demgen (2012) used this method to evaluate the feasibility of modelling trajectories in the high latitudes.

The second approach focused less on individual trajectories and more on the final density distribution. Wagner et al. (2019) used this method to indicate whether Lagrangian trajectories can simulate the spread of tracer (sometimes solved Eulerian) through the ocean and found in general that results are consistent, but care should be taken in boundary currents and (other) regions of high variations of eddy kinetic energy. Van Sebille et al. (2009) used a statistical test (two-sample Kolmogorov-Smirnov test) to evaluate whether the final distribution of two data sets was similar, in this case the final locations of drifters and modelled trajectories and found that the reliability of the outcome very much depends on the input data set and its resolution.

Thirdly, Qin et al. (2014) defined the concept of divergence time as the time it takes for two trajectories to be x kilometres apart, i.e. divergence times are high if two trajectories are similar. Their main conclusion was that in regions of high eddy kinetic energy (EKE), divergence times are small, and that divergence times shorten when temporal averaging increases.

Drifter-modelled trajectory separation in the Arctic for CMEMS

In this thesis I studied trajectory separation using the first approach described in section 3.3. Since Demgen (2012) already did an analysis of high latitude Lagrangian drifters, I used the same method and domain in order to be able to compare results. Also, the regions used were found to be the main pathways of particles travelling through ice released in the Bering Strait.

The drifter data is twelve hourly drifter data from the International Arctic Buoy Program (IABP). The buoys are sorted by buoy id and filtered based on whether the sequence was continuous in time (no gaps of more than 10 days), in space (no gaps of more than 500 km) and whether there were no anomalous speeds (of more than $20\,\mathrm{km\,h^{-1}}$), and only buoys between 2001 and 2016 were considered. The buoy trajectories are divided in two regions of interest. On the one hand, the buoys in the Fram Strait, and on the other hand the buoys in the Beaufort Gyre region (figure A.8). Trajectories were

attributed to a region if they had at least 1 point between 50°-80°N and 30°W-30°E (Fram) and with all values between 90°W-90°E and above 65°N (Beaufort). The surface velocities are known to be much higher in the Fram Strait, hence it is interesting to see the difference for the two regions. The number of drifters considered is 105 for the Fram strait and 342 for the Beaufort Gyre.

First, I released particles from the initial location and initial time derived from the buoy trajectory and sampled their location every 12 hours. I did this for the two kernels as in figure 3.2 and equation 3.1 in order to compare the difference between a relatively simple (sic) kernel and a more complex (sig) kernel with integrated seasonality. I calculated the great circle difference between the drifter trajectory and the modelled trajectory for all buoys for each available time step.

Next, to determine the 'chaos within the system' I also released virtual drifters 12 and 24 hours before and after the specific buoy release. For this set, I calculated the great circle distance to the virtual particle released at the same time as the buoy (the reference trajectory). Per region the median is shown, because it is less influenced by extremes than the mean. To illustrate this: The mean was much higher than expected when one of the (virtual) particles went into a different pathway (e.g. CAA and Fram Strait, figure A.8). Because particles cannot travel on land, this displacement did not give physically meaningful information. Furthermore, it is easy to give an uncertainty range by showing the 83rd and 17th percentile, instead of shading with the first standard deviation which sometimes gave values below zero, which are nonphysical.

3.4 Individual trajectories

This section discusses the methods uses for simulating individual trajectories of particles entering the Arctic. The releases were done daily for three years, on 10 locations in an equidistant line (figure A.9). Particles were released in the Bering Strait at 66°N and between 169° and 168.5°W. The particles in the Norwegian Sea were released at 67°N between 10° and 10.5°E. I determined the location such that the release region had a mean northward flow, based on the 16 year average currents (figure A.4). The start date was 2009-02-01 and the trajectory length was 1700 days. All particles are released and advected at the top level of the data, which is 0.5 m deep. The total number of particles per simulation was 10950. Both the releases were done with an ice+ocean kernel (the sic-kernel of before) but also with an ocean-only kernel. The ocean-only kernel only advected particles based on ocean velocities.

To analyze the trajectories the following steps were followed. First, the trajectories were visually inspected, to identify the major pathways. Then, the displacement between initial and final location along a great circle was calculated. The total amount of times the transition was calculated by

summing how often particles switched from the ocean state to the ice state. Next, the fraction of time spent in ice was calculated by dividing the number of days spent in ice by the total number of days considered. The transition from ocean to ice says more about how often a particle has been in the marginal ice zone and could have transitioned, than about how often it actually did, the sig-kernel would have been a better tool for this, but this was outside the scope of this project. Consequently, histograms were made based on the fraction of days spent in ice and number of times it transitioned from ocean to ice, both for all particles (black histograms) and for particles grouped together dependent on their location after 1700 days. The sections are shown in figure 3.3 and are divided based on 68°N. The sections were made to study connectivity between the Pacific Ocean (red histograms) and the Atlantic Ocean (green histograms) (figure 4.5 and 4.6).

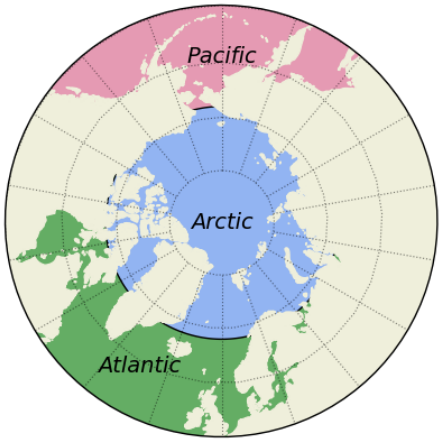

Figure 3.3: Sections used for analysis. The lower boundary for the Arctic section is at 68 North, because this is just north of the release location for the Bering strait.

3.5 Statistical accumulation

This part of the method dives deeper in how I applied the transition matrices.

Releases for the transtion matrix

The particles are released evenly spaced on a lon-lat grid from 50°N to 90°N with at least 100 particles per 1×1 degree grid cell. The particles were released on February 1st, 11th, or 21st for respectively 60, 40 and 20 days. The maximum ice extent in the Arctic (figure A.10) is in early March, hence the trajectories are set up so they are centered around the period with maximum ice extent. The particles were advected with the sic kernel from equation (3.1). The release years were 2014, 2015 and 2016, because these were the last three years available from the data set. Another

release was done for August 1st, 11th, or 21st for respectively 60, 40, and 20 days to capture the minimum sea ice extent. To test sensitivity, some simulations were done for a sharp transition between ocean and ice for a sea ice concentration of 5, 30, 60 and 95 % and also for only ocean advection.

Construction of the transition matrix

A simple example of the construction of the transition matrix is given in section 2.4. The grid used for this thesis had a resolution of one by one degree. Therefore, the matrix used for this study has depending on the resolution $14001(40 * 360 + 1)$ or $3601(20 * 180 + 1)$ columns and rows. The +1 is for an extra cell for particles leaving the domain, e.g. flowing south with the East Greenland Current. Also, two sensitivity analyses were done with resolutions of 0.5 and 2 degrees. An extra step in constructing the matrix is the removal of sinks. Sinks are cells that particles, upon entering, do not leave anymore. Only few of these cells are identified in the Canadian Arctic Archipelago and are it means that most particles get 'stuck' on land, because the flow fields used there do not perform so well with this resolution because the rossby radius of transformation is very small here (Nurser and Bacon, 2014). Sink cells are set to zero and the column is normalized afterwards.

Density evolution

The density evolution was achieved through taking the dot product of $\vec{T}$ and an initial distribution. For a homogeneous initial distribution this is vector of ones (equation (3.2)). This multiplication was iterated x times, until the density distribution hardly changes any more, based on visual inspection. In case different trajectory lengths are compared (20,40,60 days) the total time span is set beforehand to determine the different number of iteration steps.

$$v_{\vec{t=dt}} = \vec{T} \cdot \begin{bmatrix} 1 \\ \vdots \\ 1 \end{bmatrix} \tag{3.2}$$

Eigenvectors

The right eigenvectors are calculated with help of `scipy`'s sparse matrix eigenvector function. The 15 largest eigenvectors were selected and the ones with an eigenvalue of 1 or close to one, respectively stationary densities and slowly decaying attractors (after Stuart (2014)). Consequently, the main structure were identified by visual inspection and obvious outliers were ignored, i.e. the ones with

a numerical sink (due to being stuck on land) or an attractor outside the domain are not discussed explicitly in this research.

4 Results

4.1 Drifter trajectory reproduction

This section focuses on the question how good models are in representing ice movement. Models can never reproduce reality, but even with these limitations, models can still teach us things about the mechanisms behind processes and results are interpreted with these limitations in mind.

I used model output from an assimilated ocean circulation and sea ice model as input data for the Lagrangian simulations. In order to evaluate the limitations of the Lagrangian simulation and the data the following section discusses the divergence of model trajectories and observed drifter trajectories, and divergence of model trajectories among each other. It gives an indication of the trustworthiness of my results, but also results of other modelling studies using individual trajectories.

Two subdomains were extracted from the Arctic, the Beaufort Sea region and the Fram Strait region and both results were studied separately (drifters visible in figure A.8). Also the differences between the observed and virtual trajectory are studied in different plots. Furthermore, the plots show the different kernels: the sic kernel (equation (3.1)) and the sig kernel (figure 3.2) The sig kernel is expected to be a more accurate representation of the physical mechanism of capturing particles since it includes the 'seasonality' by using a pr melt and growth of sea ice.

Figure 4.1 shows the median distance between the virtual trajectories and the observed trajectories for the different kernels and the shading the 17th and 83rd percentile. The most remarkable difference is the difference in the top part of the shading. The median displacement of both regions seems to be the same (up to 200-300km), but the spread of is much higher for the Fram Strait region (figure 4.1a) than for the Beaufort Gyre region (figure figure 4.1b). The difference between the two kernels is very small for both regions.

Figure 4.2 shows the difference in distance among the different virtual trajectories: the difference between the virtual drifter released at the same time as the buoy and the virtual drifters twelve and 24 hours before and after the buoy release. Remarkable is the large difference between the two

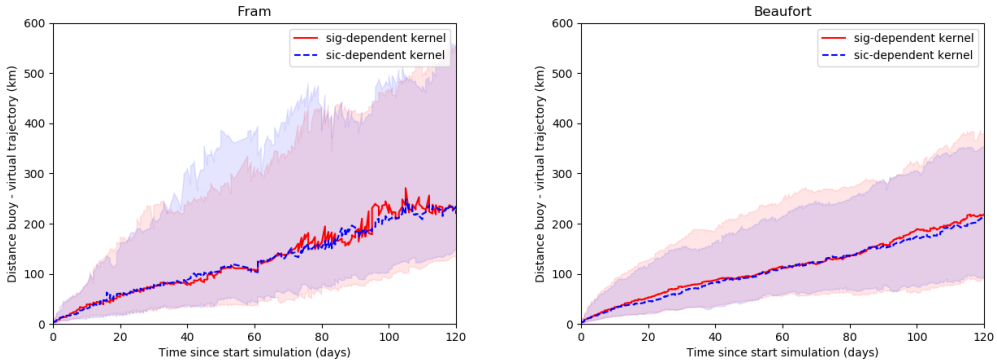

(a) (b)

Figure 4.1: Median distance between buoy trajectories and virtual trajectories for the Fram Strait region and the Beaufort Gyre region. The sea ice growth (sig) dependent kernel is schematically represented in figure 3.2 and the sea ice concentration (sic) dependent kernel is just described by equation 3.1. Shading is at 17th and 83rd percentile.

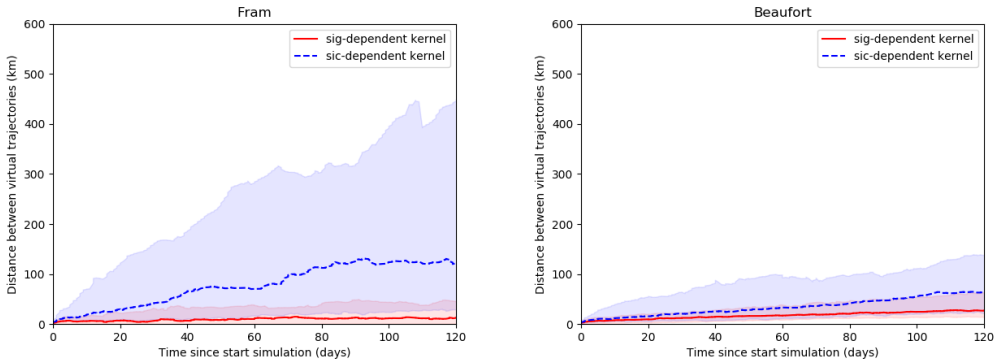

(a) (b)

Figure 4.2: Median distance among virtual trajectories in the Fram Strait region and the Beaufort Gyre region. Shading is at 17th and 83rd percentile.

different kernels. Both the median and the spread seem to be an order of magnitude larger for the sic-kernel than the the sig-kernel. The other very large difference is the magnitude of divergence between the different regions. For the sic-kernel the spread is approximately 5 times larger and the median twice as big for the distance between the particles. However, the distances between different trajectories of particles released not more than a day apart is much larger for the Fram Strait region than the Beaufort Gyre region.

Comparing figures 4.1 and 4.2 shows that the sic-kernel divergence for both among-virtual drifters (figure 4.2) and between observed and virtual drifters (figure 4.1) is of order of hundreds of kilometers. However, for the sig-dependent kernel distances are an order of magnitude less in the case of divergence of virtual drifters among each other (figure 4.2), than for divergence between observed and simulated trajectories (figure 4.1).

4.2 Individual trajectories through main gateways

In order to understand where particles come from, I modeled particles released in the main 'entrances' of the Arctic. Section 2.1 shows that in previous literature two main pathways into the Arctic are defined. The main pathways are through the Bering Strait (figure 4.3) and along the coast of Norway (figure 4.4). First of all, I interpret the pathways of particles moved by both ice and ocean. Secondly I investigate the difference between particles only advected by ocean, and by ice+ocean, aiming to learn more about transport mechanisms. The previous section shows that in ice covered regions, the divergence can be quite large, hence it is important not to look at individual trajectories, but at the main features of many particle trajectories together. For this section, all figures are produced with help of the simple sic-kernel.

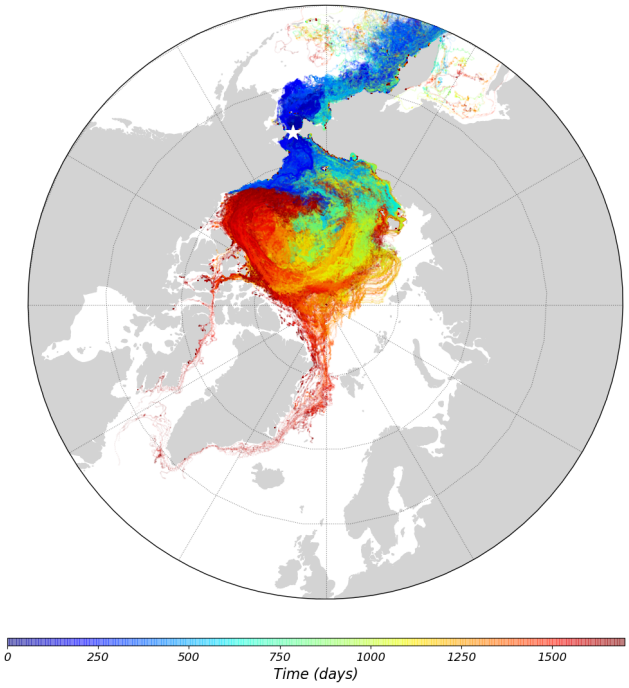

Figure 4.3: Trajectories for 1700 days after release in the Bering Strait. Release location is labeled with a white star. 10 particles are released every day for three years.

Table 4.1: Percentage particle trajectories with final location in a section (figure 3.3) depending on their final location for the ice+ocean kernel. If the particle left the domain, the last point in the domain was taken. For the releases in the Bering Strait (figure 4.3) and in front of the Norwegian coast (figure 4.4)

	Bering	**Norway**
Arctic	84.1%	64.6%
Atlantic	0.3%	35.4%
Pacific	15.6%	0.0%

Figure 4.3 shows that particles released in the Bering strait can go two ways: North into the Arctic or south into the Pacific. Most particles flow north into the Beaufort Gyre and some eventually cross the Arctic to the Atlantic Ocean. Within the time scale of the plotted trajectories, only a fraction (0.3%) of the particles reaches the Atlantic, and only after almost 5 years (table 4.1). Two pathways for reaching the Atlantic can be identified: either through the Canadian Arctic Archipelago, or through the Fram Strait and East Greenland Current.

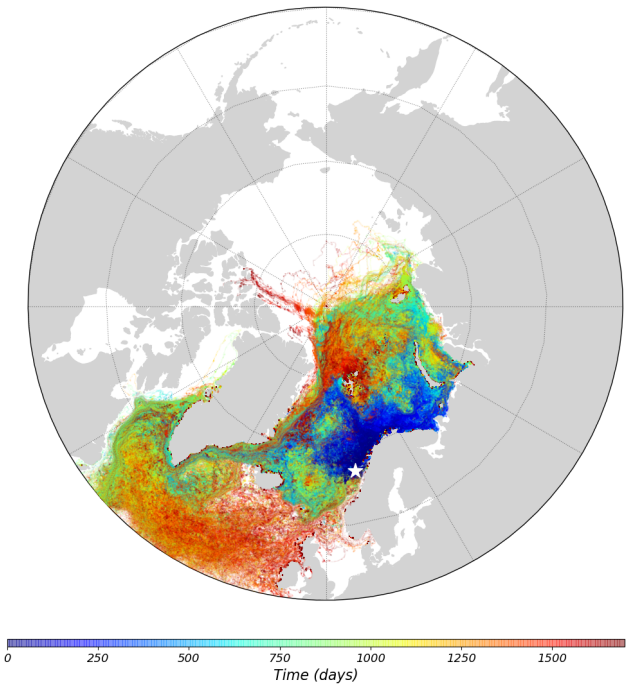

Figure 4.4: Trajectories for 1700 days after release in Norwegian Sea. Release location is labeled with a white star. 10 particles are released every day for three years.

Table 4.2: Final location per section for the 'high' Arctic. Like figure 3.3 but with the border of the Arctic Section moved northward to 80°N. Only for the release location in front of the Norwegian Coast. If the particle left the domain, the last point in the domain was taken.

	Ice + ocean	**Only ocean**
Arctic	10.4%	21.4%
Atlantic	89.2%	74.9%
Pacific	0.3%	3.7%

Particles released in the Norwegian Sea either follow the coast and pass Nova Zembla or follow the West Spitsbergen Current (figure 4.4). In the given time, only a small fraction (10.7%) of the released particles makes it way into the high Arctic (above 80°N), and none make it to the Pacific Ocean in the given time (table 4.2). The particles that did move northward seem to be 'pushed' back to the Atlantic, with the exception of a handful. Note that the division of the domain into

sections is most meaningful for distinguishing whether particles crossed the Arctic, i.e. from Norway to the Pacific Ocean and from the Bering Strait to the Atlantic Ocean, and less for distinguishing for sea ice covered parts of the Arctic versus e.g. Nordic Seas (table 4.1).

The trajectories for the only ocean release seem to travel further than the ice+ocean releases (figures A.15 and A.16). Remarkable is that a larger percentage of the Bering releases crosses the ocean relative to the ice+ocean kernel. Also, a larger percentage of the Norway release ends up in the 'Arctic' section relative to the ice+ocean kernel (table 4.3).

Table 4.3: Fraction ending up per section for only ocean kernel. If the particle left the domain, the last point in the domain was taken. For the releases in the Bering Strait (figure A.15) and in front of the Norwegian coast (figure A.16)

	Bering	**Norway**
Arctic	93.5%	72.1%
Atlantic	1.2%	27.9%
Pacific	5.3%	0.0%

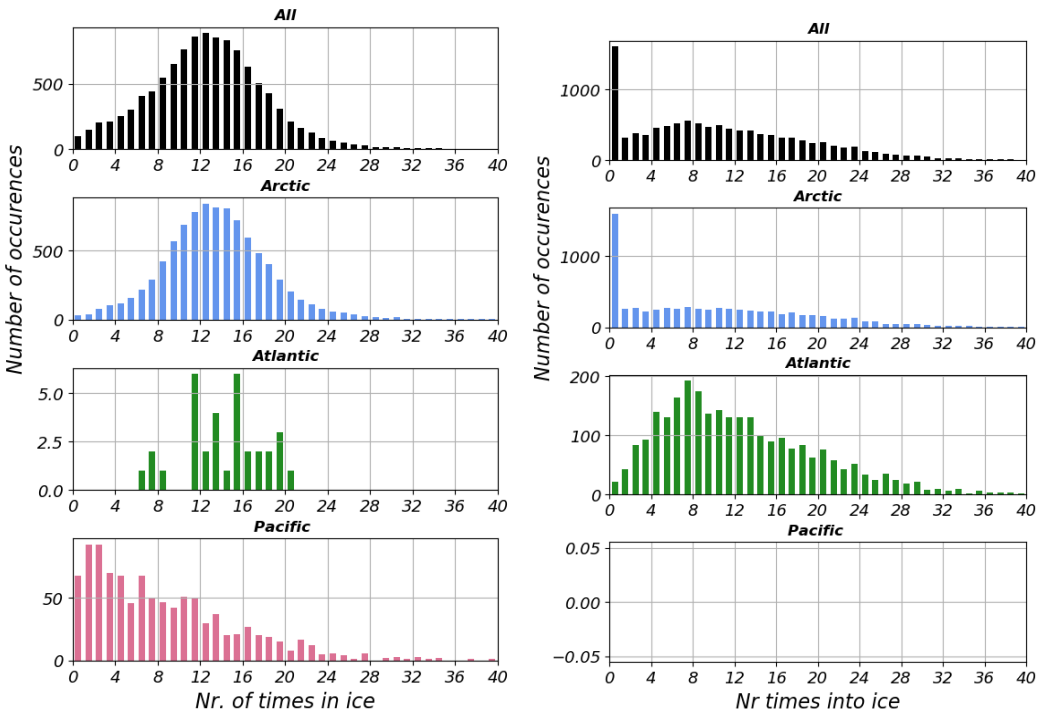

(a) Release in Bering Strait

(b) Release in Norwegian Sea

Figure 4.5: Number of times transition is made from the ocean into ice. The upper panels is for all particles and the lower panels show per location specific, depending on final location (sections shown in figure 3.3). Note the scale is different for the different plots.

Studying the trajectories of particles released gives information about the pathways of the par-

ticles, but on top of that it is also interesting to look at the mechanism of transport. What are the main drift or current patterns moving particles and what medium is most important? Figure 4.5 gives further insight how often particles made the transition from ocean to ice. The histogram is divided into different sections (shown in figure 3.3), based on the final location of the particle after 1700 days. The final locations of both the Bering Strait and the Norway release can be found in figure A.14.

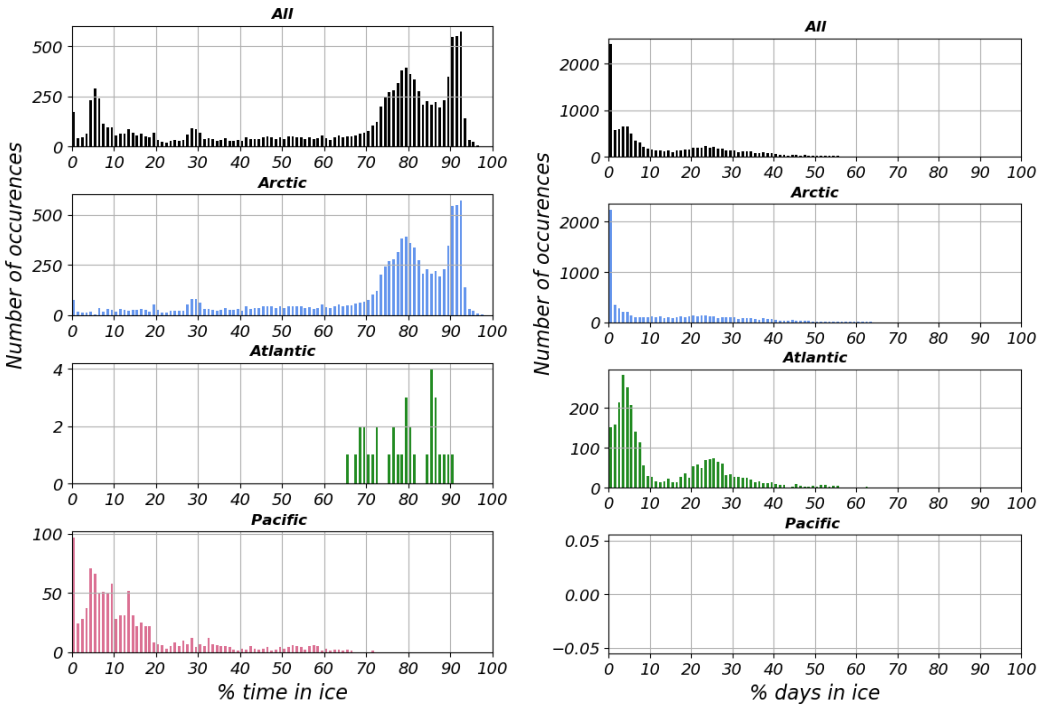

(a) Release in Bering Strait

(b) Release in Norwegian Sea

Figure 4.6: Percentage time spent in ice. The upper panels is for all particles and the lower panels show per section specific, depending on final location (sections shown in figure 3.3). Note the scale is different per section.

Figure 4.5 shows how often a particle made the transition from ocean to ice in 1700 days and figure 4.6 shows the percentage of time a virtual particle spent in ice (as a percentage of the total time). In figure 4.5a, only 33 out of 10950 particles made it into the Atlantic section (green), and most stayed in the Arctic section (blue). When a particle travels across or in the Arctic to the Atlantic, the average number of times it enters ice is much higher than when it stays in the Arctic. If it flows south into the Pacific (red) it enters the ice even less often. This is also true for the percentage of time spent in ice. Figure 4.6a shows that particles spent little time in ice when ending up in the Pacific, but if they entered the Atlantic they spent at least 60% of their time in ice, or at least within the marginal ice zone. None of the particles spent all its time in ice. For the Arctic section there are two peaks, which is not observed for the number of times they go into ice. This

might suggest two pathways.

For particles entering the Arctic Ocean from the Atlantic side, there are many particles that are not entering the sea ice (the high peak above 0 in the black panel, figure 4.5b). This is especially true for the Arctic section (blue panel). If particles travel to the Atlantic section they are very likely to have transitioned from ocean to sea ice, yet not so often as for the Bering particles released and ending up in the Atlantic or Arctic (blue and green panel in figure 4.5a).

Also the analysis of time spent in ice confirms that Atlantic particles spent no time in the ice if ending up in the Arctic Section (blue panel figure 4.6b). Note that the Arctic section entails some part of the Nordic Seas (figure A.2). On the contrary, particles ending up in the Atlantic spent some time in ice.

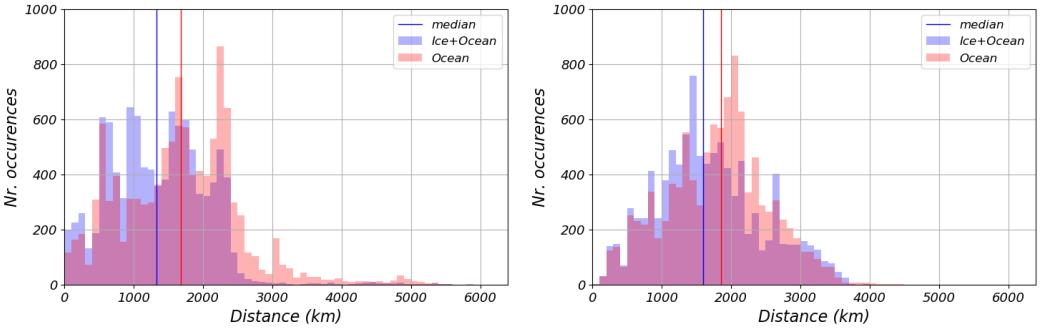

(a) Bering Strait release (b) Norway release

Figure 4.7: Comparison of distances travelled from initial location for only ocean advection and ice+ocean advection

Figure 4.7 shows the distances between the initial and final point, contrasting the ocean-only kernel with the ice+ocean kernel. This figure shows that when the particle only travels in the ocean it travels on average further than when it is also transported by ice, for both the Norwegian release as the Bering release. Note that for the Norway release, most particles do not enter ice. The two medians are closer together for the Norway release. Since this figure only shows the distance between the initial and final point, it does not say something about the path travelled and deflected particles might actually come closer to their initial point after deflection.

4.3 Accumulation patterns

From the previous figure it seems that depending on the inflow, particles end up in different parts of the (Arctic) ocean, i.e. from the Atlantic inflow, most particles do not enter the deep Arctic and from the Pacific inflow most stay in the Arctic Basin over the course of four years. It also seems that sea ice either works to transport particles into a different section of the ocean or slows the flow of particles down, e.g. from the Pacific to the Atlantic many particles are 'trapped' in the Beaufort Gyre. Therefore this section studies if particles accumulate in certain regions with help of Markov Chains. I first investigate the tracer density evolution of the whole domain and continue with identifying the eigenvectors. Then I describe the accumulation of the Beaufort Gyre and Atlantic specifically and conclude with the density evolution starting from the two main 'entrances', the Bering Strait and the Norwegian Sea. The density evolution maps the final maps of multiplying an initial distribution with the transition matrix, hence values above 1 show accumulation and values lower than 1 show divergence of tracer.

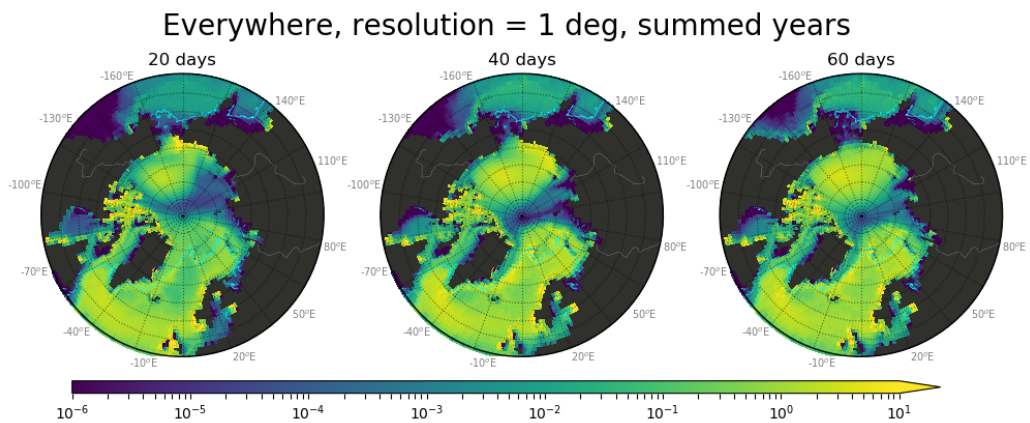

Figure 4.8: Tracer density evolution starting from a homogeneous distribution for 1 degree for the summed transition matrix for 2014, 2015, 2016. The light-blue line is the maximum sea ice edge in 2015. The map is made after 2400 days. The initial value of 1 is yellow-green, so where ever there are yellow spots there is accumulation. Note that the scale is logarithmic.

Figure 4.8 shows the final state of the tracer density of particles after 2400 days (∼6.5 years) for a transition matrix made of the summed years (a transition matrix based on all the trajectories in 2014, 2015 and 2016). The initial distribution was homogeneous with a tracer density of 1 everywhere (therefore it does not have units). Multiplying this with a transition matrix gives us the density after $x \times dt$ time steps. After 2400 days the density distribution changes little, established by visual inspection. On top of that, it is a convenient time period to compare different dt's for the

sensitivity analysis (2400 is a product of 20, 40 and 60). Figure 4.8 shows us the general patterns of accumulation and loss of mass. Some noteworthy patterns are the accumulation zones in the Beaufort and Chukchi seas and the accumulation in the Nordic Seas. It is hard to differentiate one basin in the Atlantic section that has higher accumulation than surrounding seas. On the other hand 'mass' is lost along the east coast of Greenland and in the Central Arctic. The mass loss on the east coast of Greenland is especially visible for the higher dt in the Fram Strait.

The same two accumulation features (Beaufort Gyre and Nordic Seas) are visible for different parameters used in the model. First of all, the kernel was varied for the edge of the sea ice extent, from 15% to 5, 30, 60 and 95% (shifting the steep slope in equation (3.1) and figure 3.1) and the main features are still visible (figure A.21). Differences between the 5% and 95% case are: In the Atlantic section accumulation seems to be more shifted to the south for the 95% part (red in figure A.22) and more to the Lofoten basin for the 5% case (blue in in figure A.22). The main patterns are also visible for the changing resolution of the transition matrix to either 0.5 or 2 degrees (figure A.20). In summer the accumulation in the Beaufort Gyre seems to be gone (figure A.18) and for the ocean only kernel the accumulation is less strong in the Beaufort Gyre and in the Nordic Seas.

In order to have a more elegant approach to the accumulation zones I study whether the features mentioned before also show up as attractors in the eigenvector analysis. A stationary density is defined with as an eigenvector of the transition matrix with corresponding eigenvalue 1, and they serve as an attractor. However, if the corresponding eigenvalue is not 1 exactly but close to one, it still gives information on slowly decaying attractors. It is more elegant as it shows the attractor at infinite time as opposed to stopping the density evolution after 2400 days. Figure 4.8 shows the density evolution of the summed transition matrices but figure 4.9 shows the eigenvector of the different years separately. 2015 and 2015 have an attractor in the middle of the Beaufort Gyre, but the convergence zone seems to be less strong and/or shifted to the west in 2014 (figure 4.9a).

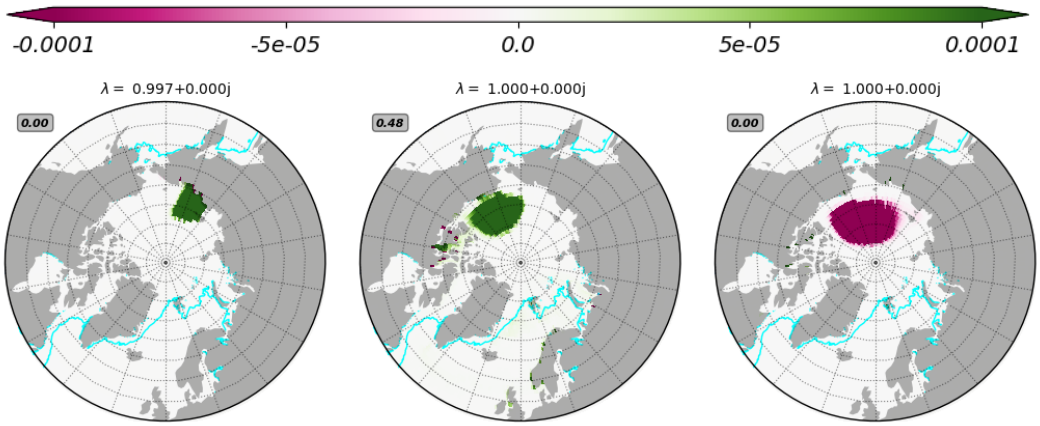

(a) 2014 (b) 2015 (c) 2016

Figure 4.9: Eigenvectors with an attractor in the Beaufort Sea, the sign of the eigenvector (the color) does not matter. The light blue line is the sea ice extent in 2015. The simulation length is 40 days and the resolution is 1 degree.

Since a strong accumulation pattern seems to be present for different years in the Pacific side of the Arctic, it is interesting to study if this feature stays robust among different dt's and resolutions and hence is not only an artifact of the method. The concept of tracer accumulation factor (TAF) is introduced, as described before in Van Sebille et al. (2012). TAF is the accumulation of tracer relative to its initial value, and in this case it has the same meaning as the value in the colorbar of figure 4.8. Figure 4.10a shows the sampling line for the tracer accumulation factor. Figure 4.10b shows the same pattern already identified in the figure 4.9 with a distinct accumulation in the Beaufort Sea for 2015 and 2016 and a smaller and more westward accumulation in 2014. This pattern is still visible for a resolution of 2 degrees and a 20 and 60 days timestep (dt), although for the lower resolution the tracer accumulation factor is lower (figure A.11c). The TAF is probably lower for 2 degrees because there is less tracer available in total (the initial value is still 1 per grid cell, but less grid cells). For the dt of 60 days for the 1 degree resolution the accumulation is higher than the 40

days dt and for the dt of 20 days the accumulation is lower (figure A.11b and A.11a respectively). In areas of lower velocities 20 days might not be enough to escape grid cells or on the other hand, lead to more numerical diffusion, which can prevent accumulation (McAdam and van Sebille, 2018).

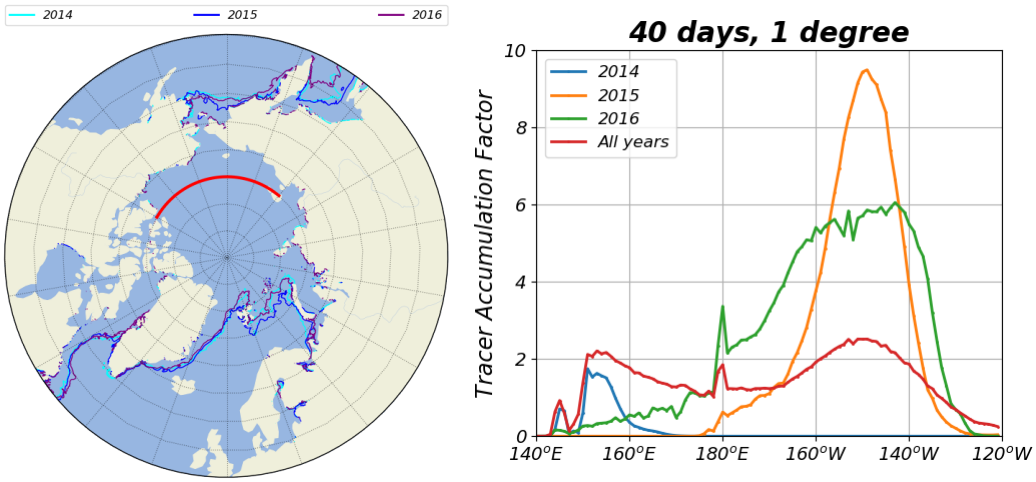

(a) (b)

Figure 4.10: a) Red line indicates the cross section for the tracer accumulation figures. The other lines are the maximum ice extent (15% concentration) for 2014-2016. b) Tracer Accumulation Factor along line in a) for 1 degree and 40 days for years 2014-2016 and the transition matrix based on the sum of the trjaectories in different years

On the Atlantic side of the domain there also was an accumulation zone visible (figure 4.8): The whole Atlantic acts as an accumulation zone. From figure 4.11 it is visible that the Atlantic Side is also an attractor for the summed years, but also for the individual years (see figure A.13). Depending on the model parameters, the attractor neatly follows the sea ice edge, except for above Nova Zembla where it slightly extends into the Central Arctic.

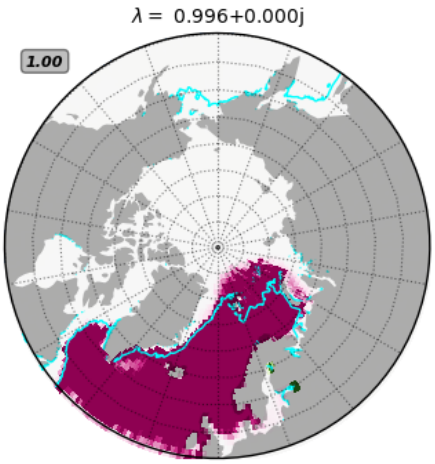

Figure 4.11: Eigenvector for simulation of 60 days, resolution 1 degree, transition matrix made for summed years

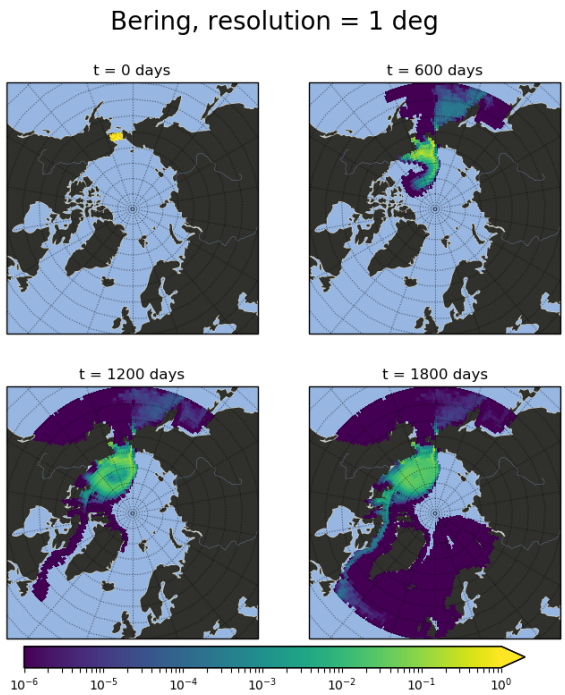

Figure 4.12: Time evolution of tracer from Bering strait. The simulation length is 60 years and is done in 2015. The grid lines are at every 20 degrees longitude and 5 degrees latitude. This particular simulation has resolution of one degree.

Apart from identifying patterns from an initial homogeneous distribution, the density evolution can be used as a different approach for individual trajectories through the main gateways. In order to see the evolution over time and not only the final distribution, different panels in time are shown. The initial density distribution was the top left panel in figures 4.13 and 4.12. Tracer on land is automatically removed within the first time step as in the transition matrices no particles are initiated on land. The patterns in figures 4.13 and 4.12 are very similar to the spread of the particles in the individual trajectories. The tracer starting in Norway hardly enters the Arctic and instead flows back into the Atlantic. Tracer starting in the Bering Strait (figure 4.12) eventually makes its way to the Atlantic Ocean, but the CAA seems to be an important pathway. Furthermore, figure 4.12 shows the time scale for particles and/or tracer to cross the Arctic, which is at least 4 years.

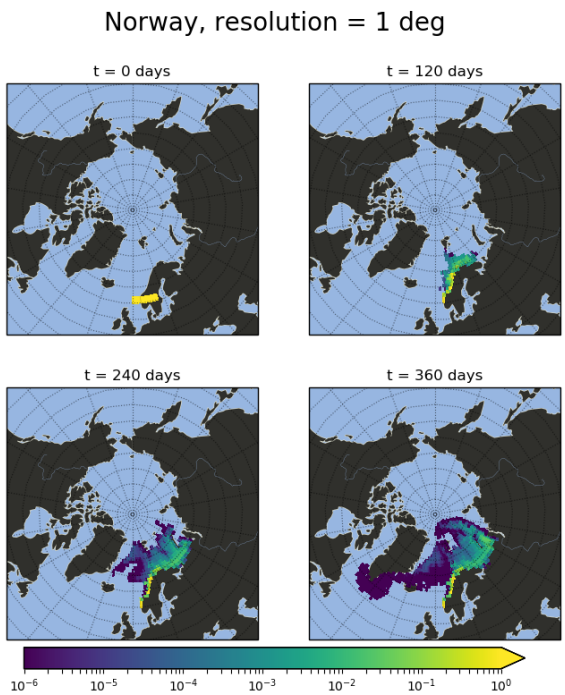

Figure 4.13: Time evolution of entrance in Norwegian Sea, for 1 degree, 60 simulation days and in 2015

5 Discussion and conclusion

First of all, in my results I found the major pathways and accumulation regions. Furthermore the results show that diffusion is high for trajectories in the Arctic. In the first part of the discussion I interpret the results. Then I consider possible limitations, to continue with putting the results in context and concluding with suggestions for future research.

Interpretation of results

This section interprets the results found in Chapter 4, by first validating the data and investigating the diffusion measured, to continue with the particle trajectories in the Arctic and finally interpreting accumulation.

Drifter diffusion

The distances between the virtual trajectories and the buoys are so large (100-550 km) that the two trajectories are hardly related any more within 120 days (figure 4.1), since estimated Rossby radii of deformations are an order of magnitude smaller (5-15 km) for different regions in the Arctic (Nurser and Bacon, 2014). It does not matter which kernel (simple: sic, or complex: sig) is used, buoy trajectories are not well reproduced with virtual drifters.

The difference between the two regions (Fram Strait and Beaufort region) for divergence of virtual drifters among each other (figures 4.2a and 4.2b) is remarkable, yet not entirely unexpected. If particles switch more often between ocean and sea ice, or stay longer in the ocean they diverge more. It seems that in the Fram Strait, more particles have switched medium (made a transition between sea ice and ocean) compared to the Beaufort Region. The sic-kernel has a larger divergence than the sig-kernel, because it is allowed to switch more often. More over, in the Fram Strait the difference between the two kernels is enhanced. This can have to do with the 15% contour line for sea ice concentration, i.e. the sea ice extent edge, is located in the Fram Strait region the whole year

(figure 2.1) and less often in the Beaufort Sea, which means the particles are more likely to switch since they are in the Marginal Ice Zone. In other words, sea ice meets warmer waters and gets more dispersed, hence there is a larger chance of particles to enter the ocean. Since particles are more likely to switch between sea ice and ocean near the sea ice extent edge, they are more prone to be picked up by different velocities and hence diverge faster in the Fram Strait. In general, I expect the ocean to have a less coherent flow than sea ice (due to e.g. eddies), hence also more divergence. Furthermore, both the sea ice and the ocean velocities are higher for the Fram Strait region (figure A.4), which is associated with a smaller divergence time (Qin et al., 2014).

Also the difference between the two kernels is very large for the among drifter divergence(figure 4.2): the distance between virtual drifters in the sic is up to 10 times larger than for the sig kernel. Since particles are less likely to switch between ocean and ice for the sig-kernel, it seems plausible that the divergence is lower for this kernel.

The comparison between figure 4.1 and figure 4.2 shows how much of the buoy-virtual particle displacement is due to internal variability. For the sic-kernel the divergence is of the same order of magnitude ($\sim$ 300 km) for both the observed-virtual trajectories (figure 4.1) and the among virtual drifters trajectories (figure 4.2). For the sig-kernel observed-virtual divergence is approximately an order of magnitude lower for the among-virtual-drifter divergence. If the distances are of the same order, it shows that if buoys themselves are not well reproduced, this can be due to the chaotic nature of the ocean-sea ice system. Only if flow field data and advection modelling would be very high in resolution the divergence could be less. However, even though this is the case for the sic-kernel, this is not entirely true for the sig kernel. Still, part of the divergence can be explained by the resolution of the data and chaos in the ocean. Because not one of the two kernels performs better in reproducing observed buoy trajectories, and the sic-kernel has less complexity and has more diffusivity, it is used for the other results. Furthermore, the results from the drifter analysis show that it is best not to look at individual trajectory of drifters.

All in all, these results show that it is very hard to interpret individual virtual trajectories, because distances are so large between virtual and observed trajectories. The general motion of virtual drifters (figures 4.3 and 4.4) corresponds to the known ocean currents. Instead of analyzing individual drifter trajectories, many paths with small disturbances should be analyzed at the same time to get an insight on the probability where particles go or originate. Furthermore, none of the two compared kernels performs better than the other in simulating observed drifter trajectories in any of the two regions. For the sic-dependent kernel the 'internal' variability of the drifters (figure 4.2) is of the same order of magnitude as the distance between the observed and virtual drifter. Only

a much better resolution in time and space could do a better job here.

Individual trajectories

From releasing the particles in the 'gateways' I identified the major pathways. First of all, I discuss the Pacific particles. The main patterns identified for particles entering from the Pacific were the Beaufort Gyre and the crossing of the Arctic to the Atlantic. Crossing the Arctic seemed to be possible in two ways, either through the Canadian Arctic Archipelago or through the Fram Strait. Even though it is tempting to say that the Fram Strait pathway is dominant, the analysis of the drifters showed that these pathways are not always well resolved: sometimes virtual drifters take another pathway than the observed did, hence more research should be done about the percentage going in both trajectories (CAA and Fram). The ocean-only particles traveled further on average and were more likely to cross the Arctic. This is somewhat surprising, because usually the ice drift velocities are larger than the ocean velocities (figure A.7). Many particles in the ice+ocean kernel stayed in the Beaufort Gyre region and together with the results from the accumulation analysis, it seems that the ice slows the particles down by possibly accumulating them in the middle of the Beaufort Gyre. Once particles are in the Canadian Arctic, the ocean currents do move them faster than the ice, so that could also be a reason for the longer distance traveled by particles in the ocean (figure A.7). Furthermore, it seems that almost all particles are captured by the ice for all sections (figure 4.5a). This is surprising for the Pacific section, but the wind could have caused southward transport of particles by blowing ice south through the Bering Strait. Particles crossing the Arctic Ocean stayed most of their time in sea ice. If you assume that (almost) all plastic is entrained by ice in the marginal ice zone, it is very likely to travel from the Pacific to the Atlantic in ice. Note however that the amount of plastic entering the Arctic from the Bering Strait is probably limited, because the amount of water entering through the Bering Strait is less than the amount of water entering the Arctic from the Atlantic Ocean, and microplastic concentrations observed in the Beaufort region are also not so high (Cózar et al. (2017); Mu et al. (2019)).

Secondly, I discuss the Atlantic Particles. Floating particles entering the Arctic from the Norwegian Current hardly entered the center of the Arctic Basin. They are either transported by the West Spitsbergen Current or the North Cape Current. Like particles from the Pacific, the ocean currents only were more efficient in transporting particles large distances, and also further into the Arctic Basin, but in general most particles were deflected back to the Atlantic. Many particles never entered the ice. This makes sense, since the Barents Sea is often ice-free (figure 2.1), and

many particles 'end' up here through the North Cape Current. In addition, particles that follow the West Spitsbergen Current are deflected back to the Atlantic (like in Hattermann et al. (2016)) or circulated in the Lofoten Basin, which is also counted as the 'Arctic' section (figure A.2). However, particles that are entrained in sea ice, north of the Barents Sea, are also transported back to the Atlantic. Particles ending in the Atlantic do spent time in ice, and this points to the fact that they are encaptured in the ice further north and are transported in ice by the Transpolar Drift Stream. This seems to point to the fact that the sea ice is an important transport mechanism for plastic: it transports plastic from the north of the Barents Sea to the Fram Strait.

Accumulation

Interpreting results of the Markov Chain analysis shows us where particles end up and accumulate, even if there are some drawbacks. The Arctic is a very complex region with interannual and decadal changes. Apart from the strong loss in sea ice volume over the past decades, the main features (Transpolar Drift Stream and Beaufort Gyre) are stronger in some years than others. Therefore, inspecting individual winters could lead to a bias, as it is possible that one just studies an anomalous year instead of the mean state. On the other hand, a 'mean' state is hard to define for an environment in transition, and in addition taking the mean velocity field over different years would cancel out eddies that are important in transport and mixing of tracers. The transition matrix experiments are useful because they isolate the contribution of the winter months (in this case 'winter' is the period around the maximum in sea ice area: February-March) to the accumulation and transport of particles. Winter is when the sea ice is extended to the largest area and therefore the transition matrix repeats the period when the influence of sea transport and accumulation mechanism is largest.

The main patterns identified from the transition matrix experiments (both the tracer density evolution and the eigenvectors) confirm that tracer, and hence particles, entering from the Pacific stay in the Beaufort Gyre and tend to accumulate there. It depends on the year where the accumulation zone on the Pacific side is concentrated. The accumulation in the Beaufort Gyre is in line with expectations as the anticyclonic movement of both ice and water forces transport to the center of the gyre. However, the location of the accumulation zone in 2014 is different and less expected, because it is further west than the other years. One of the reasons could be an anomaly in the Arctic Ocean Oscillation (AOO). In both 2014 and 2015 the Arctic Ocean Oscillation had a positive index, which is associated with an elevation in the sea level in the Canada basin and hence increased convergence, so this does not explain the unexpected behaviour (Woods Hole Oceanographic Institution, 2018). Another possible explanation could be a shift of the Beaufort Gyre westwards, and its interaction

with currents flowing over the Chukchi Plateau (through e.g. eddies and the 'waiting room') (Regan et al., 2019; Kelly et al., 2019). However, data is only available until 2014 in Regan et al. (2019), so it cannot be compared with other years. Therefore more research needs to be done on this year. All in all, over the past years, the Beaufort Gyre seems to be an important accumulation zone for floating particles, but the accumulation of plastic in this zone heavily depends on the amount of plastic flowing in through the Bering Strait.

The other main accumulation zone was found in the Atlantic Ocean. The accumulation zone ended just north of the Barents Sea: north of the sea ice edge. It seems as if the Transpolar Drift Stream (location in figure A.5) is a 'barrier' for transport of ice-carried particles further into the Arctic Basin, because this is the edge of the accumulation zone. Ocean only particle simulations do not show this sharp barrier, which confirms the suspicion that it is related to sea ice drift.

The accumulation in the rest of the basin is mostly outside the sea ice extent. To further investigate the influence of sea ice drift on the location of accumulation, it is interesting to look at the difference between particles that were picked up at different sea ice concentrations (figure A.22). Particles that left the ice more easily (in the 5% sea ice edge simulation in figure A.20 and A.22) are likely to accumulate more in the Nordic Seas between Iceland and Svalbard, e.g. Lofoten basin, where they can recirculate. The particles that were stuck in ice (95%) are more likely to be accumulate in the Fram Strait and more south in the Atlantic, transported by the East Greenland Current, originating either from the Pacific side of the Arctic Basin or from the Transpolar Drift Stream (figure A.22). To summarize, ice captures Atlantic particles and moves them further south, and if particles stay in the ocean they are more likely to accumulate elsewhere. Much more water flows into the Arctic on the Atlantic side than on the Pacific side, hence it has a much higher potential for accumulating plastic. However, Atlantic plastic is unlikely to enter the more central part of the Arctic (the high Arctic), and therefore accumulates in the Atlantic section only and does not cross to the Pacific.

Considerations and limitations

This research used several methods that had not been used before, such as finding the eigenvector for sea ice and modelling the particle transition from ocean to sea ice and the other way around. With this new and exploratory research, assumptions are made that should be taken into account when interpreting results and that could be improved upon in future research.

First of all, nobody had done experimental or numerical models on how plastic moves in and out sea ice yet. During this research I had to apply the mechanism for entraining sediments in sea ice to plastic particles. The way it is included in this thesis is a simple approach depending on sea ice concentration. Even though this simple approach is justified for this large scale modelling without many data available, many assumptions were made about the capturing of microplastic. The same kernel was also applied for drifters, even though it is probable that different mechanisms govern transitions from sea ice to ocean for (plastic) particles and drifters. Future research could look at how plastic entrained can be more accurately parametrized, if more data is available.

Secondly, the data used had its limitations. Even though it is 1/12 degree, it is not fully eddy resolving but rather eddy permitting (Nurser and Bacon, 2014). From the drifter analysis it became clear that individual trajectories are not modelled very accurately. Furthermore, the ice thickness is sometimes under- or overestimated which might lead to e.g. overestimation of ice convergence in the Beaufort Gyre (Uotila et al., 2019). However, the plastic convergence in the Beaufort Gyre is currently so large and consistent through different methods and years, that this might just affect the scale of convergence, but not the existence of the accumulation itself.

Thirdly, the Markov Chain method can also lead to numerical diffusion. The more often the transition matrix is multiplied, the more diffusion can occur, and hence leaking along pathways that do not exist in reality (McAdam and van Sebille, 2018). In order to minimize this problem, relatively long time steps of 40 and 60 days and a resolution of 1 degree were usually used for construction of the transition matrix. The 1×1 degree resolution also meant that the grid cells did not all contain the same area. Furthermore, in the analysis of the Markov Chain, sometimes visual inspection had to be applied. Even though this is a method used more often (Stuart, 2014), it would be helpful to get a more quantifiable method for this.

Finally, some physical mechanisms were ignored. In the Arctic the interaction between different water masses is known to be important, and consequently vertical motion is also important. However, since microplastics and therefore particles were assumed to float, both sinking of plastic and three dimensional velocities were not part of this model. Also biofouling was not included, even though it

is known to be important for the lifetime of floating plastic (Fazey and Ryan, 2016). Furthermore, the assumption is made that there is no source of plastic in the Arctic itself, which is not entirely true (e.g. from fishing boats or rivers), but the contribution of plastic from within the Arctic is limited, and I focused on plastic entering through the main 'gateways' (Cózar et al., 2017).

Results in context

My results establish already proposed theories on ice in the Transpolar Drift Stream as a transport vector (Bergmann et al., 2017). It does show increased concentrations in the Barents Sea, but also in other parts of the Nordic Seas and therefore is complimentary to predicted accumulation areas (Van Sebille et al., 2012). In general these results confirm that the Fram Strait, Barents Seas and other Nordic Seas can act as an accumulation area. Furthermore, it proposes that the known convergence for freshwater might also apply to microplastics, especially in sea ice. It shows that even though most water (and therefore most plastics) enters the Arctic from the Atlantic, they do not make it further than just north of the Barents Sea and hence accumulate in the Nordic Seas. Plastic found in the Beaufort Gyre, Chukchi Sea, Kara and East Siberian Sea is more likely to be from Pacific Origin. Furthermore, sea ice is important for capturing microplastics and storing it.

Most studies so far focused on the mid and low latitudes for drifter separation. However, Demgen (2012) investigated pathways of observed and virtual drifters in the Arctic based on satellite data. A comparison of Demgen's results (the displacement of virtual drifters relative to the observed buoy trajectory, figure 5.1) and figures 4.2 and 4.1 shows that the separation distance is much lower for her case, especially in the Beaufort region. A probable reason for this difference is the input data used to advect the drifters, satellite data instead of assimilated reanalysis model data, because velocities are known to be overestimated in the model data. The divergence of the among drifter trajectories is of the same order of magnitude. A study on diffusion of Lagrangian drifters in the ice pack found displacement of the order of 200 km within 30 days (Rampal et al., 2016), which is of the same order of magnitude as results found in this thesis.

From Doddridge et al. (2019), Kelly et al. (2019) and others it is known that freshwater tends to accumulate in the center of the Beaufort Gyre. The freshwater bubble in the Beaufort Gyre is not literally freshwater, but just an equivalent freshwater content. However, the term freshwater is convenient to study it. Also the floating particles in my study accumulated in the Beaufort Gyre and therefore the freshwater mechanisms can be used to understand the mechanisms behind the convergence I observed.

In my results, 2014 seems to be an outlier because the convergence zone is shifted westward. A convergence zone west of the Beaufort Gyre happened before: Kelly et al. (2019) found that over the years there has been a shift in trajectories into the Beaufort Gyre: from 1980 there trajectories from

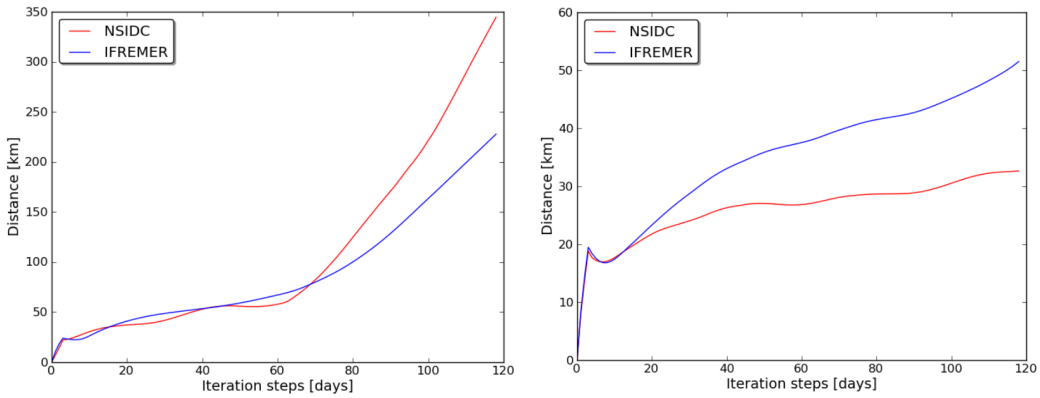

(a) Fram region (b) Beaufort region

Figure 5.1: From figure 5.8 in Demgen (2012). Note the differences in the scale. *Position uncertainties of the monthly NSIDC and IFREMER drift products for the years 1992 to 2010.*

the Pacific into the Beaufort Gyre were deflected westward and converged temporarily into a 'waiting room' before entering the Beaufort Gyre. However, this 'waiting room' disappeared in the 1990s until early 2000s. In the 2015 and 2016 accumulation zones, this waiting room is not visible, but this might be the explanation for the 2014 accumulation zone, even though the 1980-1990 'waiting room' was a bit more north. Also the shape of the Beaufort Gyre changes per year, and the 2014 accumulation zone might be due to a shift in the Beaufort Gyre (Regan et al., 2019). However, more research needs to be done.

The area north of Greenland, the second convergence zone which is found in literature (like in Kwok (2015)), is not visible as an accumulation zone in the results. Little literature is written about convergence of sea ice in the Beaufort Gyre, but the convergence area North of Greenland is not very well visible in the results, like in Kwok (2015). This absence of accumulation can have multiple causes. First of all, a few accumulation cells can be identified, yet no connected area of adjacent cells. The same feature is visible in the Canadian Arctic Archipelago, and this might be because particles get stuck on the coast here. My model has no explicit non-beaching or beaching kernel, and therefore this stuck-on-land feature does not really have a phyiscal meaning. However, that particles do get stuck is not so surprising, because this area has so many narrow and shallow straits and other complex geometry, and a rossby radius of deformation that is less than 10 km (Nurser and Bacon, 2014). The resolution of the data (1/12 degree) is probably not sufficient, but more research needs to be done. Secondly, the CMEMS GLORYS data used is known to underestimate sea ice thickness in the North Greenland region (dominated by is wind-driven convergence). Hence, it might be that this convergent motion is not well represented in data, hence also not in the results of this thesis. Finally, from A.4 it is visible that the ocean velocities are low in the region above

Greenland. Combined with figure A.7, that shows that also the ice velocities are low in this region, less transport has happened into the region in the modelled time period.

The accumulation region I found seems to be in the whole North Atlantic, including in the Barents Sea. The Barents Sea convergence has been predicted and observed (Van Sebille et al., 2012; Cózar et al., 2017) before, even though observed concentrations were lower than predicted. A possible reason for this lower concentration is that fresher surface water blocks the plastic polluted Atlantic water. Less dense surface water forces the saltier, hence denser, Atlantic water down. This can act on top of the Transpolar Drift Stream barrier that was found. Bergmann et al. (2017) found relatively high concentrations of plastic in the Fram Strait in the deep ocean, with the highest plastic concentrations at their southernmost station. My results are based on surface flow, and not on velocities deep in the ocean. However, my results show that particles are entrained in ice north of the Barents Sea and then transported to the Fram Strait, which confirms the mechanism proposed by Bergmann et al. (2017). The increasing concentrations more southward can be a result of melting sea ice as it meets the warmer Atlantic water.

My results predicted high plastic concentrations in the Beaufort Gyre. One study found relatively higher concentrations of plastic in surface water in the Chukchi Sea (located next to the Beaufort Gyre) compared to seas south of the Bering Strait (Mu et al., 2019). On the other hand papers such as Cózar et al. (2017) did not find high concentrations of plastic on the Pacific side of the Arctic compared to the Atlantic, but the values found in the Chukchi sea were orders of magnitude lower. Therefore it can still be a 'local' accumulation zone. Furthermore, Barrows et al. (2018) found that most plastic is found in the 'open' ocean and not near the coast, which was the Cózar et al. (2017) expedition. What's more the amount of accumulation depends on multiple factors: First of all, how much water flows in: more water flows in on the Atlantic side than on the Pacific side (9.5 Sv and 1.5 Sv respectively) (Kanhai et al., 2018). Secondly, on the the particle density of the inflowing water. Thirdly, on the amount of accumulation in a certain area. So it is possible that there is accumulation of plastic in the Beaufort Gyre, and specifically in the ice. However, concentrations in the Beaufort Gyre can be high compared to other seas on the Pacific Side, but they are probably still low compared to Atlantic concentrations.

Concluding remarks

In this thesis, I studied the interconnectivity between oceans through the Arctic. Individual drifters or ice cores are hard to track with reanalysis data. The general movements are still approximated well, but the divergence time for virtual and observed trajectories is very short for both the Beaufort Gyre region and especially in the Fram Strait. Part of the divergence can be explained by the intrinsic chaos of the ocean ice system, but part is due to the data used in the model.

The other findings are related to where particles end up and originate. First of all, I found that floating particles from the Pacific enter the Beaufort Gyre and usually stay there for a few years. Then they might accumulate there or cross the Arctic to the East Greenland Current and end south to the Atlantic (0.3 % of the particles transported by ice). Only a small percentage takes the route through the Canadian Arctic Archipelago and none take the route through the Nares Strait in my simulation. Along the way to the Atlantic the floating particles spent 65-90% of their time in ice and therefore ice seems to be an important vector for transport. Secondly, floating particles from the Atlantic stay in the Atlantic. They 'accumulate' in the Barents Sea or flow back via another route to a more southern part of the Atlantic Ocean. Since the observations of plastic in the Barents Sea are not as high as expected from modelling studies, some other mechanisms are expected to play a role. From my simulation it seems that if they enter sea ice, the Transpolar Drift Stream takes them to the Fram Strait where the sea ice melts and releases its particles. The Transpolar Drift Stream acts as a barrier for microplastics entering the high Arctic. Thirdly, there seem to be two accumulation regions in the Arctic. The first is the Beaufort Gyre region, but the position of the accumulation zone depends on the year. Microplastic concentrations in water in the Chukchi sea were higher than seas more to the south, yet still orders of magnitude lower than other regions in the Arctic (Cózar et al., 2017; Mu et al., 2019). It must be noted that these observations were done in the surface ocean, while the high concentrations were especially predicted in sea ice. The other accumulation area seems to be the Atlantic part, extending from the Barents sea to the other Nordic Seas.

All in all, Arctic plastic is more likely to come from the Pacific and travel at least part of the time through ice. Ice is important for the distribution of microplastic by acting as a barrier, transport vector or as a temporary sink.

Outlook

This thesis led to more question than it answered. First of all, in order to better understand the sources of plastic in the Arctic it is important to learn more about the concentrations flowing in through the main 'entrances'. Currently, the virtual particles could not be linked to actual amounts of microplastic entering the Arctic and therefore microplastic measurements need to be taken in e.g. the Bering Strait. Secondly, further research could look into how to improve the individual trajectory method to get an insight in the probable origin of ice cores or plastic. Important is that one should take into account that the diffusion of ice can be quite high, also shown in this thesis, and therefore it is hardly possible to find a single origin. Therefore this research could focus on a probabilistic approach to origins of for example cores. Thirdly, another ice velocity data set can be used for ice transport, because studies have shown that satellite derived velocities gives better estimations for velocities, and moreover for sea ice thickness, which is very important for con- and divergence of ice. Furthermore, it would be interesting to study how microplastic is captured by ice, how this process can be parametrized. This would mean numerical and experimental research, investigating e.g. whether it is possible to find which sizes of microplastic are most efficiently entrained by sea ice and how efficient this capturing is. In addition, the increased stress in sea ice might contribute to fragmentation of microplastic and this could be a topic of study too. This study just looked at two-dimensional surface flow, and the Arctic is a complex system with interacting water masses and as a result three-dimensional motion is important. Therefore, a beneficial extension of this research could try to take threedimensional flow into account, combined with sinking of plastic, and compare results with deep sea/sediment measurements. Another line of research worth pursuing is the difference in transport between only ocean and combined ice and ocean transport. This thesis found that the ice north of the Barents Sea works as barrier, but that this is not true for the ocean, and I am curious if this would also be visible in other studies, and moreover, why the convergence in the Beaufort Gyre is stronger for sea ice than for ocean. In addition, an interesting line of future research could be to construct the transition matrix for the Markov Chain, drifter paths can be used. The advantage would be that actual trajectories would be studied, even though the drawback would be that the contrast between summer and winter would be harder, as well as other temporal variation. Additionally, this thesis looked at just three years, and further investigation could consider more years to find out if and how patterns and pathways are influenced by interannual and decadal changes. Finally, more measurements must be done in the Arctic in general, especially in sea ice. It would be interesting to see if the higher microplastic concentrations predicted in Beaufort Gyre sea

ice are also found in reality.

All in all, this thesis only made me wonder more about the problem of plastic in sea ice. Ultimately, chasing plastic in the Arctic is an entertaining activity, and informative when studying oceanography, but it would be best if we could prevent plastic from entering the ocean altogether.

Acknowledgements

I would like to thank all people who helped during the process of my master thesis.

https://tinyurl.com/climphys-anneke-acknow

Bibliography

D. Barnes, F. Galgani, R. C. Thompson, and M. Barlaz. Accumulation and fragmentation of plastic debris in global environments. *Philosophical transactions of the Royal Society of London. Series B, Biological sciences*, 364(1526):1985–98, jul 2009. ISSN 1471-2970. doi: 10.1098/rstb.2008.0205.

A. P. Barrows, S. E. Cathey, and C. W. Petersen. Marine environment microfiber contamination: Global patterns and the diversity of microparticle origins. *Environmental Pollution*, 237:275–284, 2018. ISSN 18736424. doi: 10.1016/j.envpol.2018.02.062. URL `https://doi.org/10.1016/j.envpol.2018.02.062`.

K. Bedi, D. Gómez-Ullate, A. Izquierdo, and T. F. Montblanc. Validating ocean general circulation models via lagrangian particle simulation and data from drifting buoys. In J. M. F. Rodrigues, P. J. S. Cardoso, J. Monteiro, R. Lam, V. V. Krzhizhanovskaya, M. H. Lees, J. J. Dongarra, and P. M. Sloot, editors, *Computational Science – ICCS 2019*, pages 253–264, Cham, 2019. Springer International Publishing. ISBN 978-3-030-22747-0.

M. Bergmann, V. Wirzberger, T. Krumpen, C. Lorenz, S. Primpke, M. B. Tekman, and G. Gerdts. High Quantities of Microplastic in Arctic Deep-Sea Sediments from the HAUSGARTEN Observatory. *Environmental Science & Technology*, 51(19):11000–11010, 10 2017. ISSN 0013-936X. doi: 10.1021/acs.est.7b03331. URL `http://pubs.acs.org/doi/10.1021/acs.est.7b03331`.

S. Bouillon, M. A. Morales Maqueda, V. Legat, and T. Fichefet. An elastic–viscous–plastic sea ice model formulated on Arakawa B and C grids. *Ocean Modelling*, 27(3-4):174–184, 1 2009. ISSN 1463-5003. doi: 10.1016/J.OCEMOD.2009.01.004. URL `https://www-sciencedirect-com.proxy.library.uu.nl/science/article/pii/S1463500309000043`.

S. Bouillon, T. Fichefet, V. Legat, and G. Madec. The elastic-viscous-plastic method revisited. *Ocean Modelling*, 71(2):2–12, 2013. ISSN 14635003. doi: 10.1016/j.ocemod.2013.05.013.

S. Chatterjee, R. P. Raj, L. Bertino, O. Skagseth, M. Ravichandran, and O. M. Johannessen. Role

of greenland sea gyre circulation on atlantic water temperature variability in the fram strait. *Geophysical Research Letters*, 45(16):8399–8406, 2018. doi: 10.1029/2018GL079174.

M. Chevallier, G. C. Smith, F. Dupont, J. F. Lemieux, G. Forget, Y. Fujii, F. Hernandez, R. Msadek, K. A. Peterson, A. Storto, T. Toyoda, M. Valdivieso, G. Vernieres, H. Zuo, M. Balmaseda, Y. S. Chang, N. Ferry, G. Garric, K. Haines, S. Keeley, R. M. Kovach, T. Kuragano, S. Masina, Y. Tang, H. Tsujino, and X. Wang. Intercomparison of the Arctic sea ice cover in global ocean–sea ice reanalyses from the ORA-IP project. *Climate Dynamics*, 49(3):1–30, 2017. ISSN 14320894. doi: 10.1007/s00382-016-2985-y.

M. Cole, P. Lindeque, C. Halsband, and T. S. Galloway. Microplastics as contaminants in the marine environment: A review. *Marine Pollution Bulletin*, 62(12):2588 – 2597, 2011. ISSN 0025-326X. doi: https://doi.org/10.1016/j.marpolbul.2011.09.025. URL `http://www.sciencedirect.com/science/article/pii/S0025326X11005133`.

A. Cózar, E. Martí, C. M. Duarte, J. García-de Lomas, E. Van Sebille, T. J. Ballatore, V. M. Eguíluz, J. Ignacio González-Gordillo, M. L. Pedrotti, F. Echevarría, R. Troublè, and X. Irigoien. The Arctic Ocean as a dead end for floating plastics in the North Atlantic branch of the Thermohaline Circulation. *Science Advances*, 3(4):1–9, 2017. ISSN 23752548. doi: 10.1126/sciadv.1600582.

S. F. Daly. Evolution of Frazil Ice. In M. Jasek, editor, *Proceedings of the 19th IAHR International Symposium on Ice. USING NEW TECHNOLOGY TO UNDERSTAND WATER-ICE INTERACTION"*, pages 29–50, Vancouver, 2008. International Association of Hydraulic Engineering and Research. ISBN 9780981044606.

D. A. Darby, W. B. Myers, M. Jakobsson, and I. Rigor. Modern dirty sea ice characteristics and sources : The role of anchor ice. *Journal of Geophysical Research*, 116(September), 2011. doi: 10.1029/2010JC006675.

M. Demgen. Lagrangian sea ice motion derived from Eulerian satellite products compared with in-situ drift trajectories. Master's thesis, Universität Hamburg, 2012.

E. W. Doddridge, G. Meneghello, J. Marshall, J. Scott, and C. Lique. A Three-way Balance in The Beaufort Gyre: The Ice-Ocean Governor, Wind Stress, and Eddy Diffusivity. *Journal of Geophysical Research: Oceans*, page 2018JC014897, 2019. ISSN 2169-9275. doi: 10.1029/2018JC014897. URL `https://onlinelibrary.wiley.com/doi/abs/10.1029/2018JC014897`.

M. Drévillon, C. Régnier, J.-M. Lellouche, G. Garric, C. Bricaud, O. Hernandez, and Approval.

Quality information document For Global Ocean Reanalysis Products GLOBAL-REANALYSIS-PHY-001-030, 2018.

F. M. Fazey and P. Ryan. Biofouling on buoyant marine plastics: An experimental study into the effect of size on surface longevity. *Environmental Pollution*, 210:354–360, 03 2016. doi: 10.1016/j.envpol.2016.01.026.

F. Fetterer, K. Knowles, W. N. Meier, M. Savoie, and A. K. Windnagel. Sea Ice Index, Version 3, updated daily 2017. URL `https://nsidc.org/data/g02135`.

T. Fichefet and M. A. Maqueda. Sensitivity of a global sea ice model to the treatment of ice thermodynamics and dynamics. *Journal of Geophysical Research: Oceans*, 102(C6):12609–12646, 1997. ISSN 21699291. doi: 10.1029/97JC00480.

J. Frias and R. Nash. Microplastics: Finding a consensus on the definition. *Marine Pollution Bulletin*, 138:145–147, 11 2018. doi: 10.1016/j.marpolbul.2018.11.022.

G. Froyland, R. M. Stuart, and E. van Sebille. How well-connected is the surface of the global ocean? *Chaos*, 24(3):1–10, 2014. ISSN 10541500. doi: 10.1063/1.4892530.

T. Hattermann, P. E. Isachsen, W.-J. von Appen, J. Albretsen, and A. Sundfjord. Eddy-driven recirculation of atlantic water in fram strait. *Geophysical Research Letters*, 43(7):3406–3414, 2016. doi: 10.1002/2016GL068323.

W. D. Hibler III. A Dynamic Thermodynamic Sea Ice Model. *Journal of Physical Oceanography*, 9 (4):815–846, 7 1979. ISSN 0022-3670. doi: 10.1175/1520-0485. URL `http://journals.ametsoc.org/doi/abs/10.1175/1520-0485%281979%29009%3C0815%3AADTSIM%3E2.0.CO%3B2`.

E. C. Hunke and J. Dukowicz. An elastic-viscous-plastic model for sea ice dynamics. *Journal of Physical Oceanography*, 27(Hibler 1979):1849–1867, 1997. URL `http://journals.ametsoc.org/doi/pdf/10.1175/1520-0485(1997)027%3C1849%3AAEVPMF%3E2.0.CO%3B2`.

IPCC. *Climate Change 2013: The Physical Science Basis. Contribution of Working Group I to the Fifth Assessment Report of the Intergovernmental Panel on Climate Change*. Cambridge University Press, Cambridge, United Kingdom and New York, NY, USA, 2013. ISBN ISBN 978-1-107-66182-0. doi: 10.1017/CBO9781107415324. URL `www.climatechange2013.org`.

J. R. Jambeck, R. Geyer, C. Wilcox, T. R. Siegler, M. Perryman, A. Andrady, R. Narayan, and K. L. Law. Plastic waste inputs from land into the ocean. *Science*, 347(6223):768–771, 2015. ISSN

0036-8075. doi: 10.1126/science.1260352. URL https://science.sciencemag.org/content/347/6223/768.

L. D. K. Kanhai, K. Gårdfeldt, O. Lyashevska, M. Hassellöv, R. C. Thompson, and I. O'Connor. Microplastics in sub-surface waters of the Arctic Central Basin. *Marine Pollution Bulletin*, 130 (October 2017):8–18, 2018. ISSN 18793363. doi: 10.1016/j.marpolbul.2018.03.011. URL https://doi.org/10.1016/j.marpolbul.2018.03.011.

S. Kelly, A. Proshutinsky, E. Popova, Y. Aksenov, and A. Yool. On the origin of Water Masses in the Beaufort Gyre. *Journal of Geophysical Research: Oceans*, pages 0–3, 2019. ISSN 21699275. doi: 10.1029/2019JC015022. URL http://doi.wiley.com/10.1029/2019JC015022.

T. Krumpen, R. Gerdes, C. Haas, S. Hendricks, A. Herber, V. Selyuzhenok, L. Smedsrud, and G. Spreen. Recent summer sea ice thickness surveys in Fram Strait and associated ice volume fluxes. *Cryosphere*, 10(2):523–534, 2016. ISSN 19940424. doi: 10.5194/tc-10-523-2016.

R. Kwok. Sea ice convergence along the Arctic coasts of Greenland and the Canadian Arctic Archipelago: Variability and extremes (1992-2014). *Geophysical Research Letters*, 42(18):7598–7605, 2015. ISSN 19448007. doi: 10.1002/2015GL065462.

R. Kwok and G. F. Cunningham. Contribution of melt in the Beaufort Sea to the decline in Arctic multiyear sea ice coverage: 1993-2009. *Geophysical Research Letters*, 37(20):1–5, 2010. ISSN 00948276. doi: 10.1029/2010GL044678.

R. Kwok, G. Spreen, and S. Pang. Arctic sea ice circulation and drift speed: Decadal trends and ocean currents. *Journal of Geophysical Research: Oceans*, 118:2408–2425, 2013. ISSN 21699291. doi: 10.1002/jgrc.20191.

M. Lange and E. van Sebille. Parcels v0.9: Prototyping a Lagrangian ocean analysis framework for the petascale age. *Geoscientific Model Development*, 10(11):4175–4186, 2017. doi: 10.5194/gmd-10-4175-2017.

G. A. Maykut. Energy exchange over young sea ice in the central Arctic. *Journal of Geophysical Research*, 83(C7):3646–3658, 1978. doi: 10.1029/jc083ic07p03646.

R. McAdam and E. van Sebille. Surface Connectivity and Interocean Exchanges From Drifter-Based Transition Matrices. *Journal of Geophysical Research: Oceans*, 123(1):514–532, 1 2018. ISSN 21699275. doi: 10.1002/2017JC013363. URL http://doi.wiley.com/10.1002/2017JC013363.

J. Mu, S. Zhang, L. Qu, F. Jin, C. Fang, X. Ma, W. Zhang, and J. Wang. Microplastics abundance and characteristics in surface waters from the Northwest Pacific, the Bering Sea, and the Chukchi Sea. *Marine Pollution Bulletin*, 143(February):58–65, 2019. ISSN 18793363. doi: 10.1016/j.marpolbul.2019.04.023. URL `https://doi.org/10.1016/j.marpolbul.2019.04.023`.

L. Nouel. Global Ocean Physics Reanalysis GLORYS12V1, 2012. URL `https://sextant.ifremer.fr/record/c0635fc4-07d3-4309-9d55-cfd3e6aa788b/`.

D. Nürnberg, I. Wollenburg, D. Dethleff, H. Eicken, H. Kassens, T. Letzig, E. Reimnitz, and J. Thiede. Sediments in Arctic sea ice: Implications for entrainment, transport and release. *Marine Geology*, 119(3-4):185–214, 1994. ISSN 00253227. doi: 10.1016/0025-3227(94)90181-3.

A. J. G. Nurser and S. Bacon. The rossby radius in the arctic ocean. *Ocean Science*, 10(6):967–975, 2014. doi: 10.5194/os-10-967-2014. URL `https://www.ocean-sci.net/10/967/2014/`.

R. W. Obbard. Microplastics in Polar Regions: The role of long range transport. *Current Opinion in Environmental Science & Health*, 1:24–29, 2018. ISSN 24685844. doi: 10.1016/j.coesh.2017.10.004. URL `https://doi.org/10.1016/j.coesh.2017.10.004`.

R. W. Obbard, S. Sadri, Y. Q. Wong, A. A. Khitun, I. Baker, and R. C. Thompson. Global warming releases microplastic legacy frozen in Arctic Sea ice. *Earth's Future*, 2(6):315–320, 2014. ISSN 23284277. doi: 10.1002/2014EF000240. URL `http://doi.wiley.com/10.1002/2014EF000240`.

V. Onink, D. Wichmann, P. Delandmeter, and E. van Sebille. The role of ekman currents, geostrophy, and stokes drift in the accumulation of floating microplastic. *Journal of Geophysical Research: Oceans*, 124(3):1474–1490, 2019. doi: 10.1029/2018JC014547. URL `https://agupubs.onlinelibrary.wiley.com/doi/abs/10.1029/2018JC014547`.

C. L. Parkinson, D. J. Cavalieri, P. Gloersen, H. J. Zwally, and J. C. Comiso. Arctic sea ice extents, areas, and trends, 1978–1996. *Journal of Geophysical Research: Oceans*, 104(C9):20837–20856, 1999. doi: 10.1029/1999JC900082.

I. Peeken, M. Bergmann, G. Gerdts, C. Katlein, T. Krumpen, S. Primpke, and M. Tekman. Microplastics in the Marine Realms of the Arctic with Special Emphasis on Sea Ice. Technical report, Alfred Wegener Institute, Helmholtz Center for Polar and Marine Research, Bremerhaven, Germany, 2018a. URL `https://arctic.noaa.gov/Report-Card/Report-Card-2018/ArtMID/7878/ArticleID/787/Microplastics-in-the-Marine-Realms-of-the-Arctic-with-Special-Emphasis-on-Sea-Ice`.

I. Peeken, S. Primpke, B. Beyer, J. Gütermann, C. Katlein, T. Krumpen, M. Bergmann, L. Hehemann, and G. Gerdts. Arctic sea ice is an important temporal sink and means of transport for microplastic. *Nature Communications*, 9(1), 2018b. ISSN 20411723. doi: 10.1038/s41467-018-03825-5. URL `http://dx.doi.org/10.1038/s41467-018-03825-5`.

S. L. Pfirman, H. Eicken, D. Bauch, and W. F. Weeks. The potential transport of pollutants by Arctic sea ice. *Science of the Total Environment*, 159(2-3):129–146, 1995. ISSN 00489697. doi: 10.1016/0048-9697(95)04174-Y.

A. Proshutinsky and R. Krishfield. In a Spin: New Insights into the Beaufort Gyre. *Eos*, 100, 4 2019. ISSN 2324-9250. doi: 10.1029/2019EO119765. URL `https://eos.org/editors-vox/in-a-spin-new-insights-into-the-beaufort-gyre`.

A. Proshutinsky, R. Krishfield, M.-L. Timmermans, J. Toole, E. Carmack, F. McLaughlin, W. J. Williams, S. Zimmermann, M. Itoh, and K. Shimada. Beaufort Gyre freshwater reservoir: State and variability from observations. *Journal of Geophysical Research*, 114:1–25, 2009. ISSN 0148-0227. doi: 10.1029/2008jc005104.

X. Qin, E. van Sebille, and A. Sen Gupta. Quantification of errors induced by temporal resolution on Lagrangian particles in an eddy-resolving model. *Ocean Modelling*, 76:20–30, 2014. ISSN 14635003. doi: 10.1016/j.ocemod.2014.02.002. URL `http://dx.doi.org/10.1016/j.ocemod.2014.02.002`.

P. Rampal, S. Bouillon, J. Bergh, and E. Ólason. Arctic sea-ice diffusion from observed and simulated Lagrangian trajectories. *The Cryosphere*, 10(4):1513–1527, 7 2016. ISSN 1994-0424. doi: 10.5194/tc-10-1513-2016. URL `https://www.the-cryosphere.net/10/1513/2016/`.

H. C. Regan, C. Lique, and T. W. Armitage. The Beaufort Gyre Extent, Shape, and Location Between 2003 and 2014 From Satellite Observations. *Journal of Geophysical Research: Oceans*, 124(2):844–862, 2019. ISSN 21699291. doi: 10.1029/2018JC014379.

E. Reimnitz, J. R. Clayton, E. W. Kempema, J. R. Payne, and W. S. Weber. Interaction of rising frazil with suspended particles: tank experiments with applications to nature. *Cold Regions Science and Technology*, 21(2):117–135, 1993. ISSN 0165232X. doi: 10.1016/0165-232X(93)90002-P.

B. Rudels. Arctic Ocean circulation, processes and water masses: A description of observations and ideas with focus on the period prior to the International Polar Year 2007-2009. *Progress in Oceanography*, 132:22–67, 2015. ISSN 00796611. doi: 10.1016/j.pocean.2013.11.006. URL `http://dx.doi.org/10.1016/j.pocean.2013.11.006`.

I. Simmonds. Comparing and contrasting the behaviour of Arctic and Antarctic sea ice over the 35 year period 1979-2013. *Annals of Glaciology*, 56(69):18–28, 2015. ISSN 02603055. doi: 10.3189/2015AoG69A909.

L. H. Smedsrud. Frazil-ice entrainment of sediment: large-tank laboratory experiments. *Journal of Glaciology*, 47(158):461–471, 2001. ISSN 0022-1430. doi: 10.3189/172756501781832142.

L. H. Smedsrud. A model for entrainment of sediment into sea ice by aggregation between frazil-ice crystals and sediment grains. *Journal of Glaciology*, 48(160):51–61, 2002. ISSN 00221430. doi: 10.3189/172756502781831520.

G. Spreen, R. Kwok, and D. Menemenlis. Trends in Arctic sea ice drift and role of wind forcing: 1992-2009. *Geophysical Research Letters*, 38(19):1–6, 2011. ISSN 00948276. doi: 10.1029/2011GL048970.

R. M. Stuart. *Metastable Sets in Open Dynamical Systems and Substochastic Markov Chains*. PhD thesis, University of New South Wales, 2014.

T. Tsubouchi, S. Bacon, Y. Aksenov, A. C. Naveira Garabato, A. Beszczynska-Möller, E. Hansen, L. de Steur, B. Curry, and C. M. Lee. The arctic ocean seasonal cycles of heat and freshwater fluxes: Observation-based inverse estimates. *Journal of Physical Oceanography*, 48(9):2029–2055, 2018. doi: 10.1175/JPO-D-17-0239.1.

P. Uotila, H. Goosse, K. Haines, M. Chevallier, A. Barthélemy, C. Bricaud, J. Carton, N. Fučkar, G. Garric, D. Iovino, F. Kauker, M. Korhonen, V. S. Lien, M. Marnela, F. Massonnet, D. Mignac, K. A. Peterson, R. Sadikni, L. Shi, S. Tietsche, T. Toyoda, J. Xie, and Z. Zhang. An assessment of ten ocean reanalyses in the polar regions. *Climate Dynamics*, 52(3-4):1613–1650, 2019. ISSN 14320894. doi: 10.1007/s00382-018-4242-z. URL `http://dx.doi.org/10.1007/s00382-018-4242-z`.

M. van der Mheen, C. Pattiaratchi, and E. van Sebille. Role of indian ocean dynamics on accumulation of buoyant debris. *Journal of Geophysical Research: Oceans*, 124(4):2571–2590, 2019. doi: 10.1029/2018JC014806. URL `https://agupubs.onlinelibrary.wiley.com/doi/abs/10.1029/2018JC014806`.

E. Van Sebille, P. J. van Leeuwen, A. Biastoch, C. N. Barron, and W. P. de Ruijter. Lagrangian validation of numerical drifter trajectories using drifting buoys: Application to the Agulhas system. *Ocean Modelling*, 29(4):269–276, 2009. ISSN 14635003. doi: 10.1016/j.ocemod.2009.05.005.

E. Van Sebille, M. H. England, and G. Froyland. Origin, dynamics and evolution of ocean garbage patches from observed surface drifters. *Environmental Research Letters*, 7(4), 2012. ISSN 17489326. doi: 10.1088/1748-9326/7/4/044040.

E. Van Sebille, C. Wilcox, L. Lebreton, N. Maximenko, B. D. Hardesty, J. A. van Franeker, M. Eriksen, D. Siegel, F. Galgani, and K. L. Law. A global inventory of small floating plastic debris. *Environmental Research Letters*, 10(12), 2015.

E. Van Sebille, S. M. Griffies, R. Abernathey, T. P. Adams, P. Berloff, A. Biastoch, B. Blanke, E. P. Chassignet, Y. Cheng, C. J. Cotter, E. Deleersnijder, K. Döös, H. F. Drake, S. Drijfhout, S. F. Gary, A. W. Heemink, J. Kjellsson, I. M. Koszalka, M. Lange, C. Lique, G. A. MacGilchrist, R. Marsh, C. G. Mayorga Adame, R. McAdam, F. Nencioli, C. B. Paris, M. D. Piggott, J. A. Polton, S. Rühs, S. H. Shah, M. D. Thomas, J. Wang, P. J. Wolfram, L. Zanna, and J. D. Zika. Lagrangian ocean analysis: Fundamentals and practices. *Ocean Modelling*, 121(July 2016):49–75, 2018. ISSN 14635003. doi: 10.1016/j.ocemod.2017.11.008.

M. Vancoppenolle, T. Fichefet, H. Goosse, S. Bouillon, G. Madec, and M. A. M. Maqueda. Simulating the mass balance and salinity of Arctic and Antarctic sea ice. 1. Model description and validation. *Ocean Modelling*, 27(1-2):33–53, 2009. ISSN 14635003. doi: 10.1016/j.ocemod.2008.10.005. URL `http://dx.doi.org/10.1016/j.ocemod.2008.10.005`.

M. K. Viršek, M. N. Lovšin, Š. Koren, A. Kržan, and M. Peterlin. Microplastics as a vector for the transport of the bacterial fish pathogen species Aeromonas salmonicida. *Marine Pollution Bulletin*, 125(1-2):301–309, 2017. ISSN 18793363. doi: 10.1016/j.marpolbul.2017.08.024.

P. Wagner, S. Rühs, F. U. Schwarzkopf, I. M. Koszalka, and A. Biastoch. Can Lagrangian Tracking Simulate Tracer Spreading in a High-Resolution Ocean General Circulation Model? *Journal of Physical Oceanography*, 49(5):1141–1157, 2019. ISSN 0022-3670. doi: 10.1175/jpo-d-18-0152.1.

W. F. Weeks and W. D. Hibler. *On Sea Ice*. University of Alaska Press, Fairbanks, UNITED STATES, 2010. ISBN 9781602231016.

Woods Hole Oceanographic Institution. Arctic Ocean Oscillation Index (AOO): Beaufort Gyre Exploration Project, Oct 2018. URL `https://www.whoi.edu/page.do?pid=66578`.

S. L. Wright and F. J. Kelly. Plastic and human health: A micro issue? *Environmental Science & Technology*, 51(12):6634–6647, 2017. doi: 10.1021/acs.est.7b00423. URL `https://doi.org/10.1021/acs.est.7b00423`. PMID: 28531345.

Z. Zhang and J. C. Moore. Chapter 9 - Data Assimilation. In Z. Zhang and J. C. Moore, editors, *Mathematical and Physical Fundamentals of Climate Change*, pages 291–311. Elsevier, Boston, 2015. ISBN 978-0-12-800066-3. doi: https://doi.org/10.1016/B978-0-12-800066-3.00009-7. URL http://www.sciencedirect.com/science/article/pii/B9780128000663000097.

A | Supplementary figures

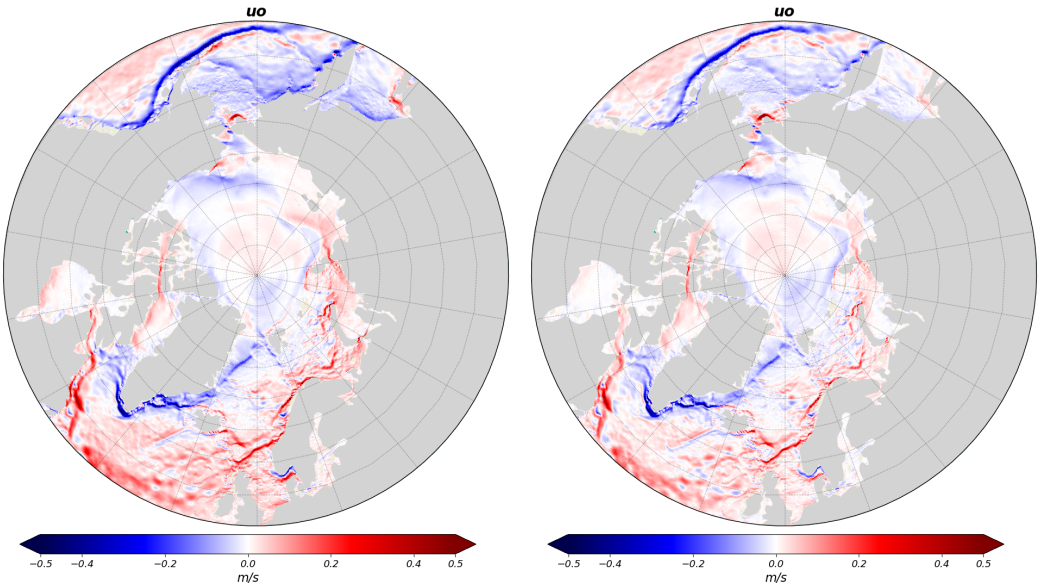

(a) DJF

(b) MAM

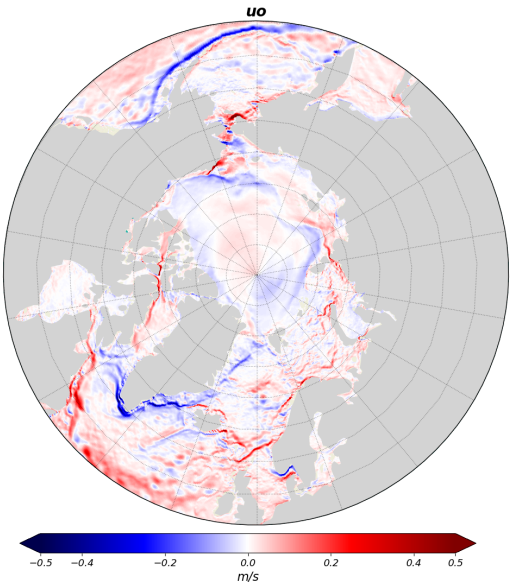

(c) JJA

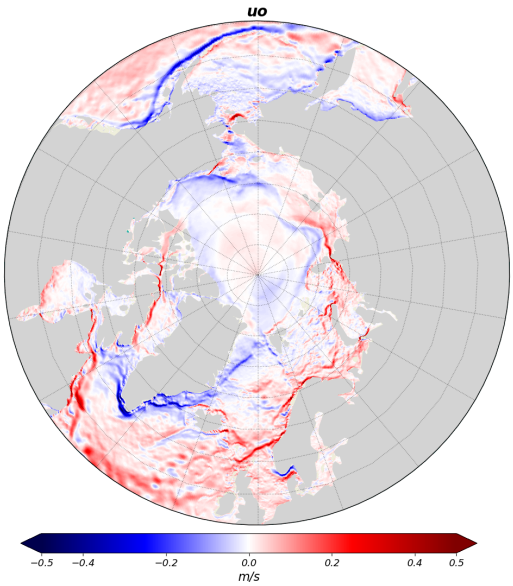

(d) SON

Figure A.1: Mean eastward ocean velocity (m/s) per season from 2001-2016

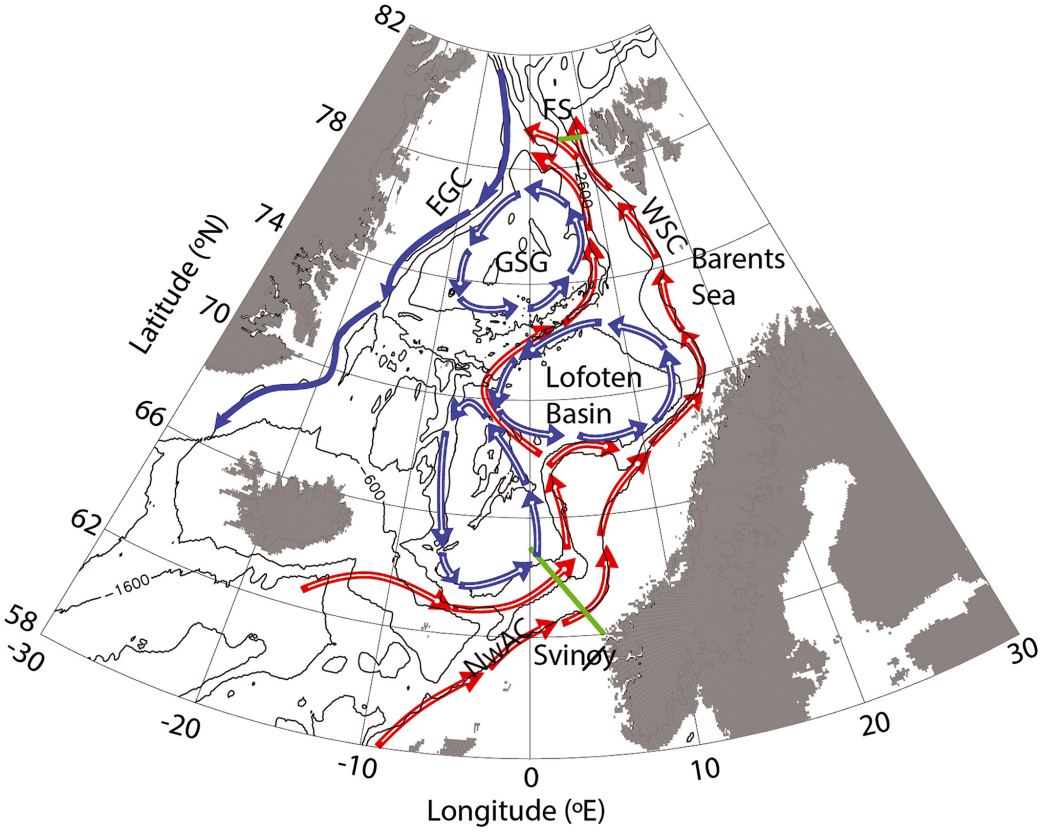

Figure A.2: Figure 1 from Chatterjee et al. (2018). *Schematic of major currents in the Nordic Seas. The red arrows indicate the Atlantic Water pathways, while the hollow blue arrows indicate the gyre circulations. The solid blue line shows the polar water flow in the East Greenland Current. Location of vertical sections, Fram Strait (79 N, 5–9 E) and Svinøy (62–65 N, 5–0 W), are indicated with green lines. The contours indicate the bottom topography with contour interval 1,000 m.*

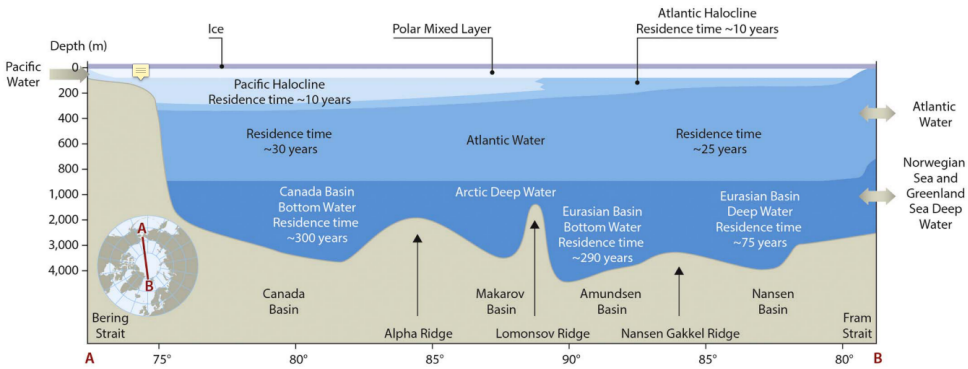

Fig. 1. General overview of the bathymetry and water masses of the Arctic Central Basin [reprinted here with permission from CAFF], (CAFF, 2013).

Figure A.3: Water masses, figure 1 from Kanhai et al. (2018) *eneral overview of the bathymetry and water masses of the Arctic Central Basin [reprinted here with permission from CAFF]*

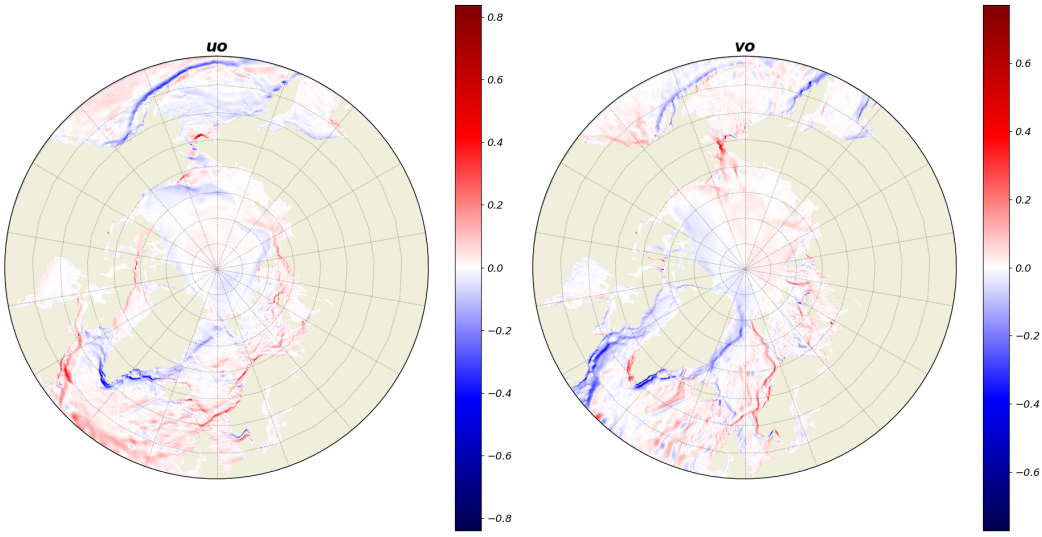

(a) Eastward velocity (m/s) (b) Northward velocity (m/s)

Figure A.4: Ocean velocities averaged from 2001-2016

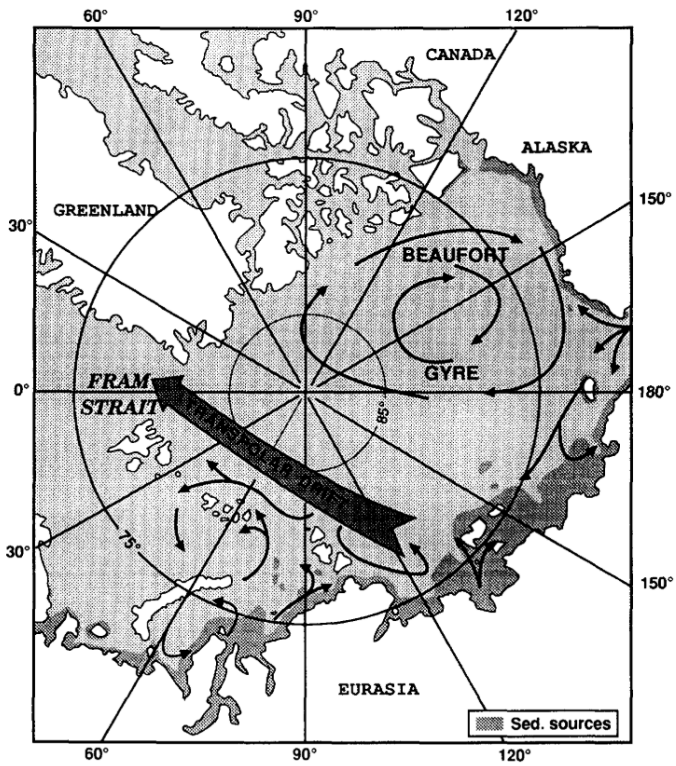

Figure A.5: Ice drift pattern, figure 1 from Nürnberg et al. (1994) *Ice drift pattern in the Arctic Ocean, after Gordienko and Laktionov (1969), with surrounding shallow (< 30 m), potential sediment source areas (stippled).*

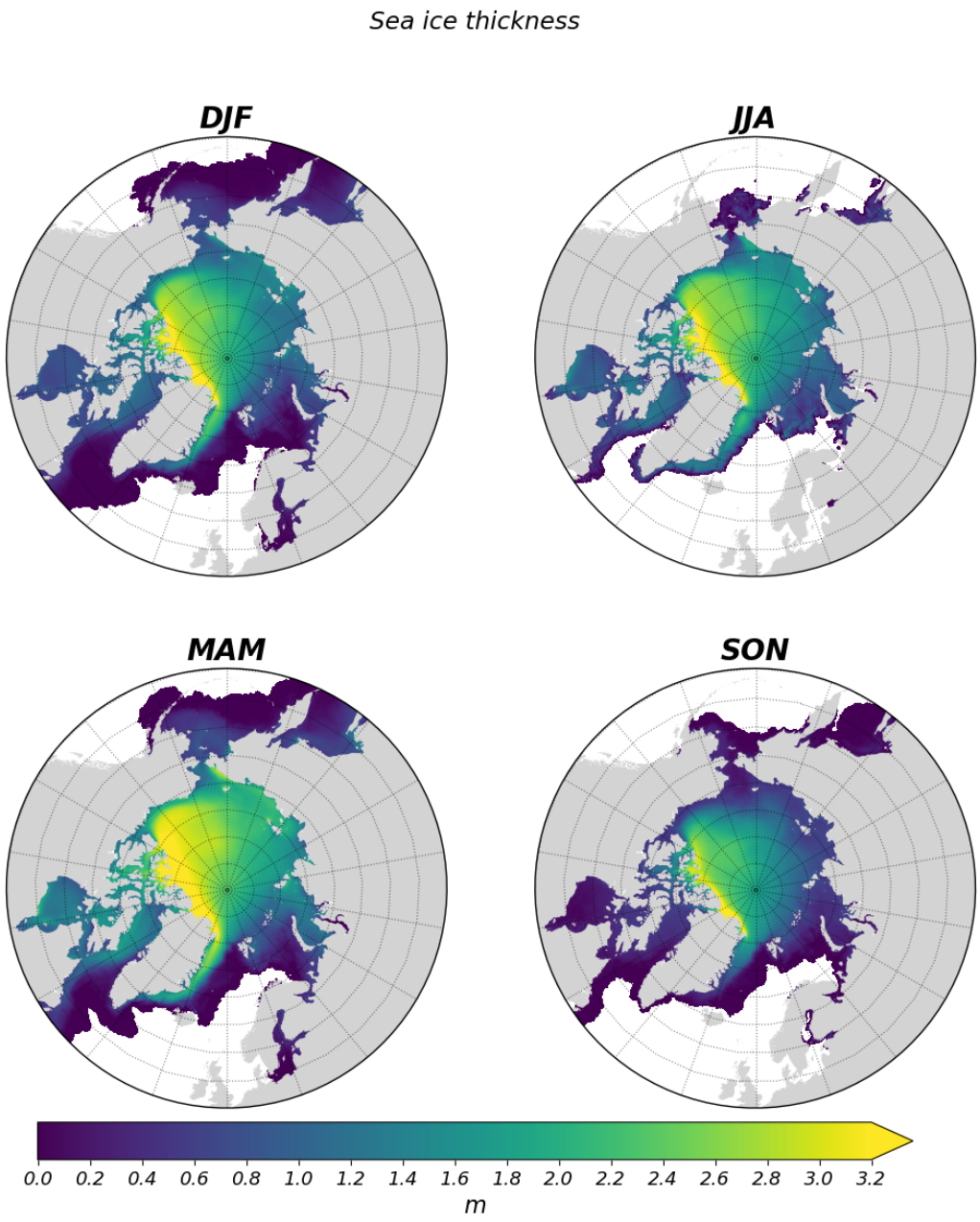

Figure A.6: Mean sea ice thickness per season over the period 2001-2016

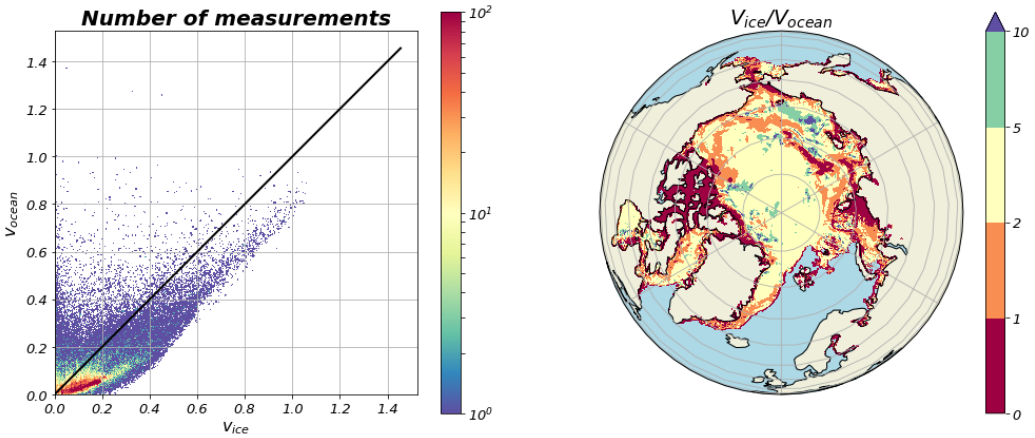

Figure A.7: Velocities of sea ice relative to ocean velocities

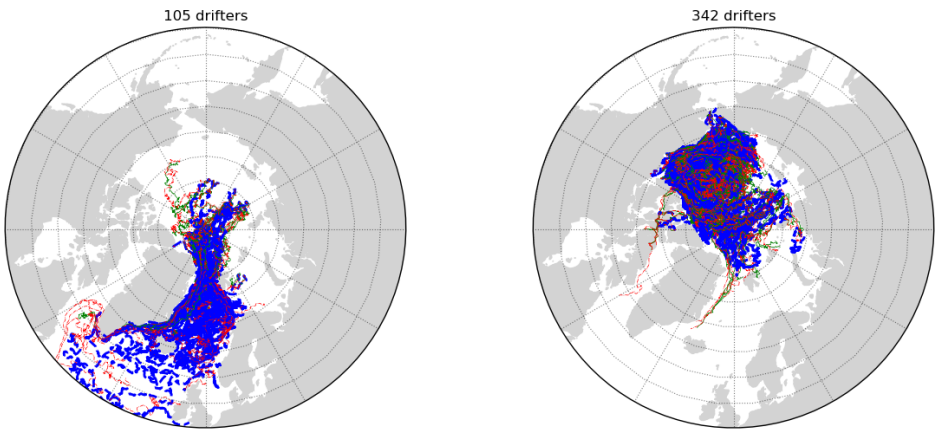

(a) Fram strait region

(b) Beaufort region

Figure A.8: The pathways of the drifters per region. The blue pathways are the original drifters and red and green the old and new kernel respectively.

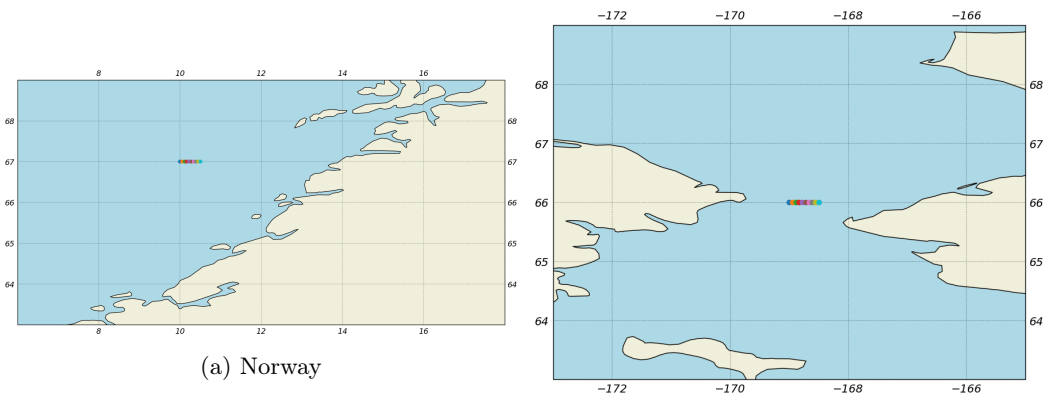

(a) Norway

(b) Bering

Figure A.9: Release locations for 10 particles per day

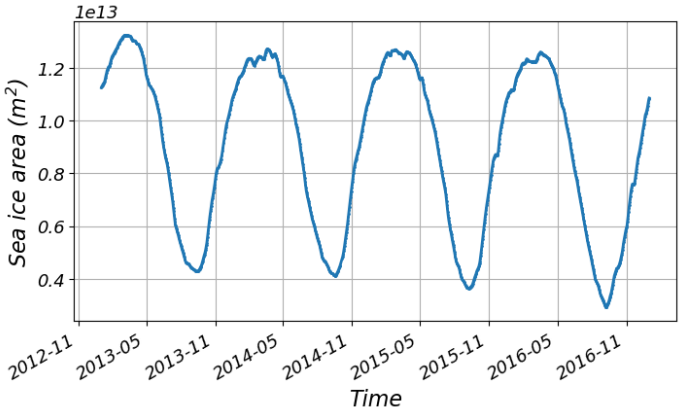

Figure A.10: Sea ice area

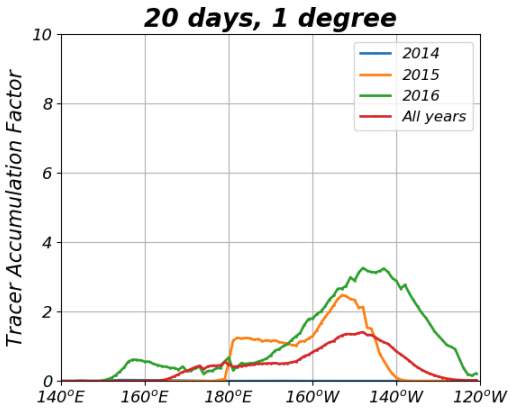

(a) TAF 1 degree, 20 days

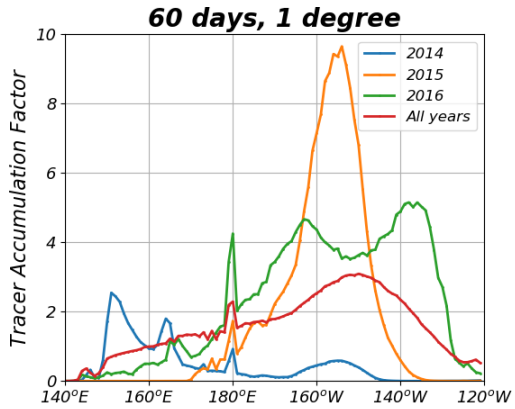

(b) TAF 1 degree, 60 days

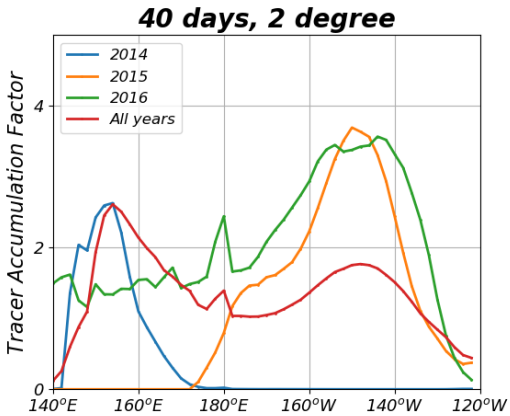

(c) TAF 2 degree, 40 days

Figure A.11: Tracer accumulation factor for different parameters

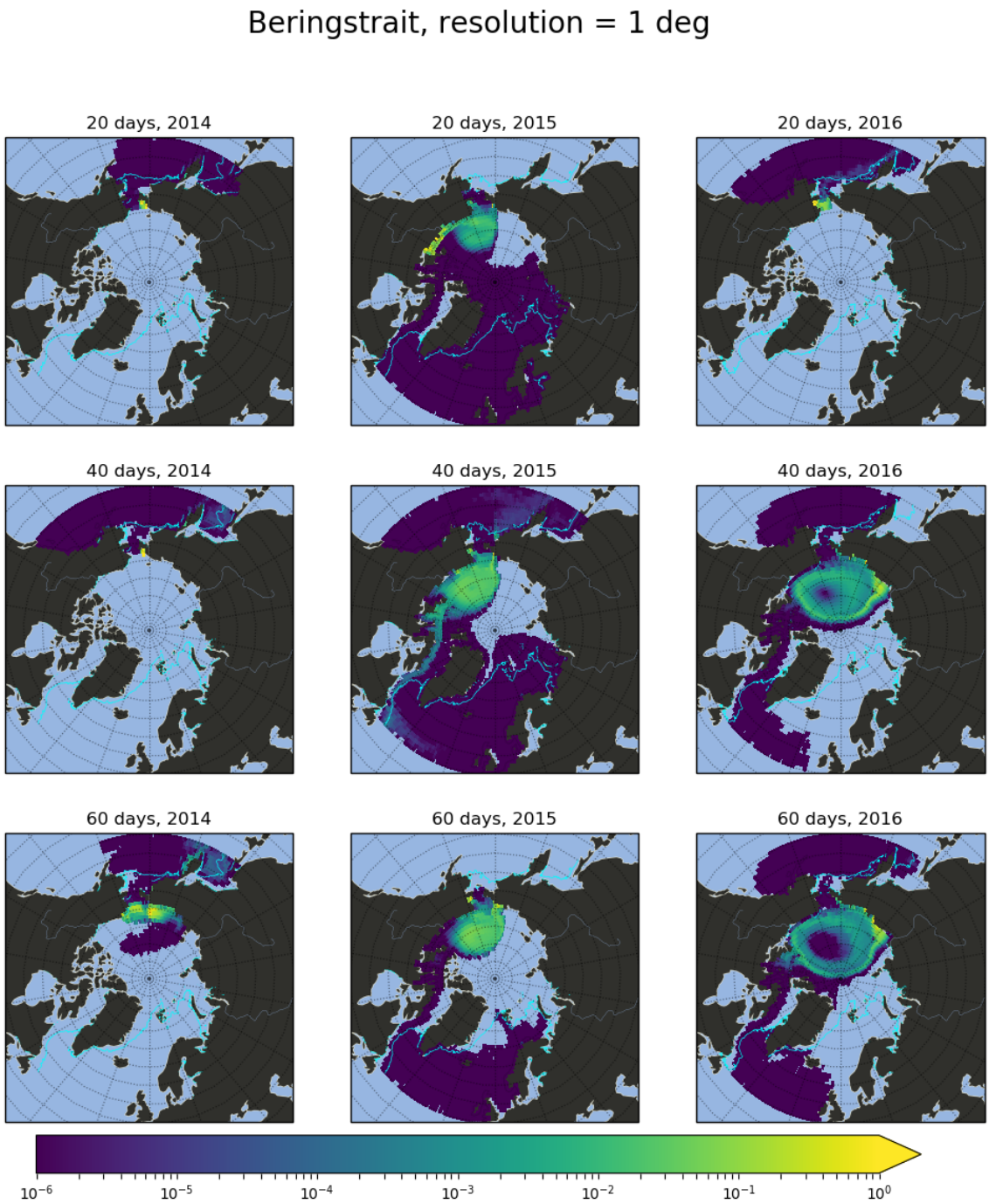

Figure A.12: The distribution of tracer after 1800 days, starting from the Bering strait. The bright blue line is the ice extent on March 1 of the mentioned year. The number of days indicate the length of the trajectory used to calculate the transition matrix. The 60 days one starts at February 1, the 40 days on February 11, and the 20 days one on February 21.

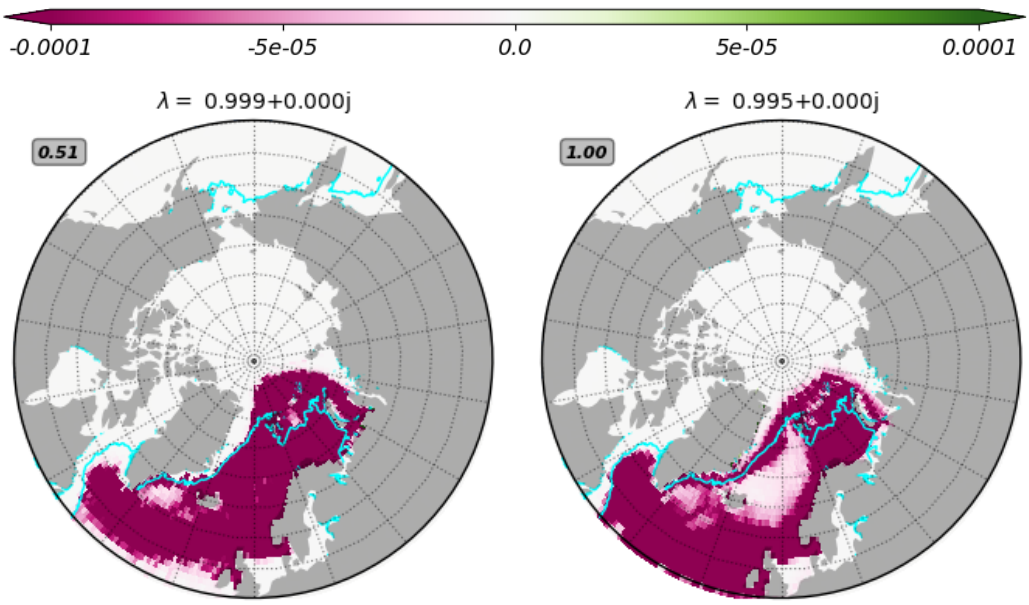

(a) 40 days, 2015, 1 degree

(b) 20 days, 2014, 1 degree

Figure A.13: Eigenvectors with an attractor in the Norwegian Sea

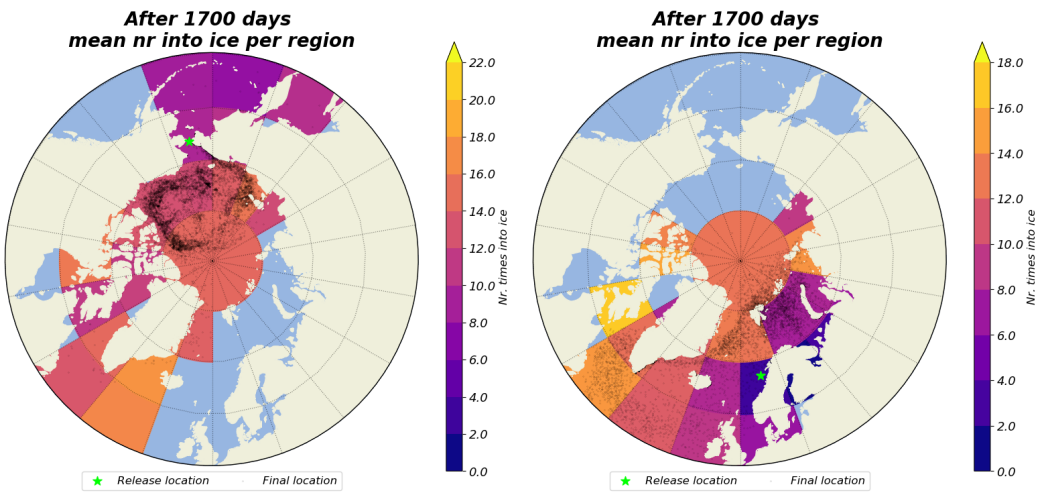

(a)

(b)

Figure A.14: Final distributions. Black dots are final location

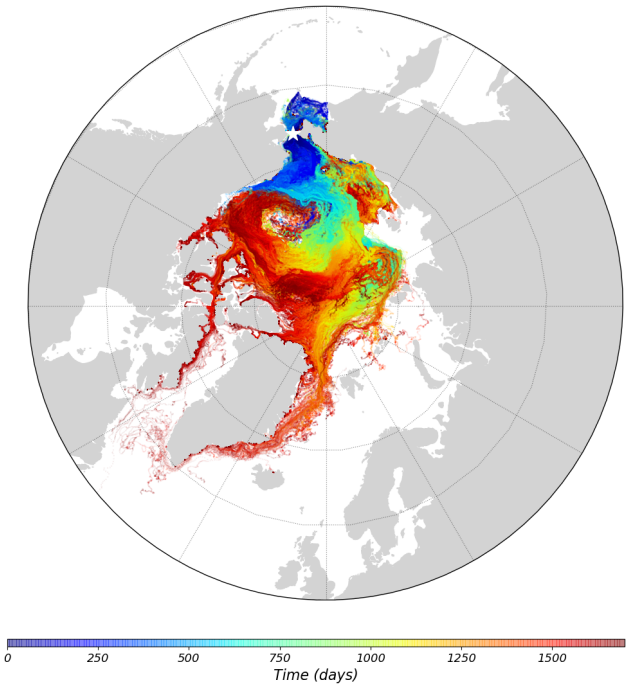

Figure A.15: Trajectories for 1700 days after release in Bering strait. Release location is labeled with a white star. 10 particles are released every day for three years. Only with advection in ocean.

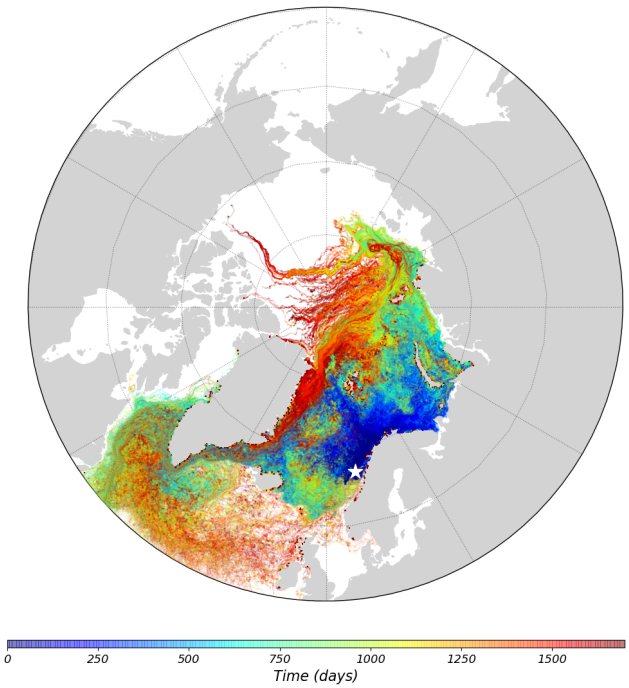

Figure A.16: Trajectories for 1700 days after release in Norwegian sea. Release location is labeled with a white star. 10 particles are released every day for three years. Only with advection in ocean.

A.1 Sensitivity

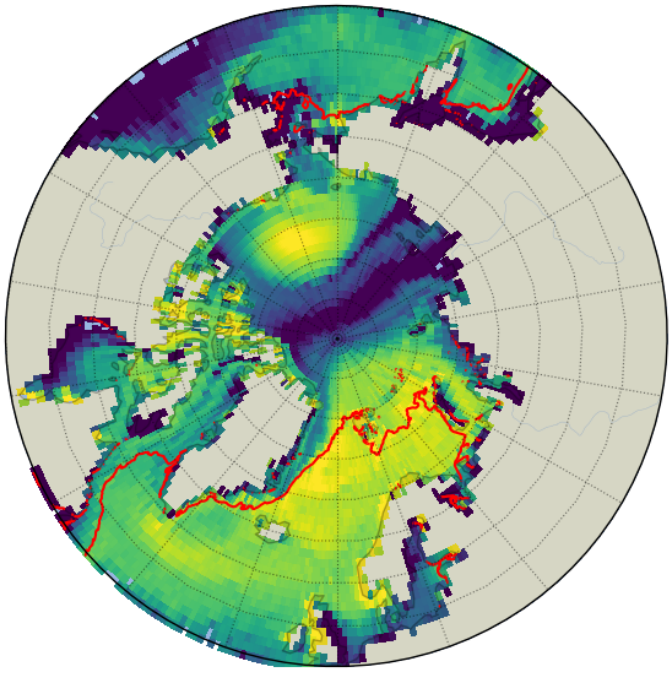

Figure A.17: Original: density evolution after 2400 days, for 1 degree and kernel switch for 15%. Transition matrix made in winter 2015.

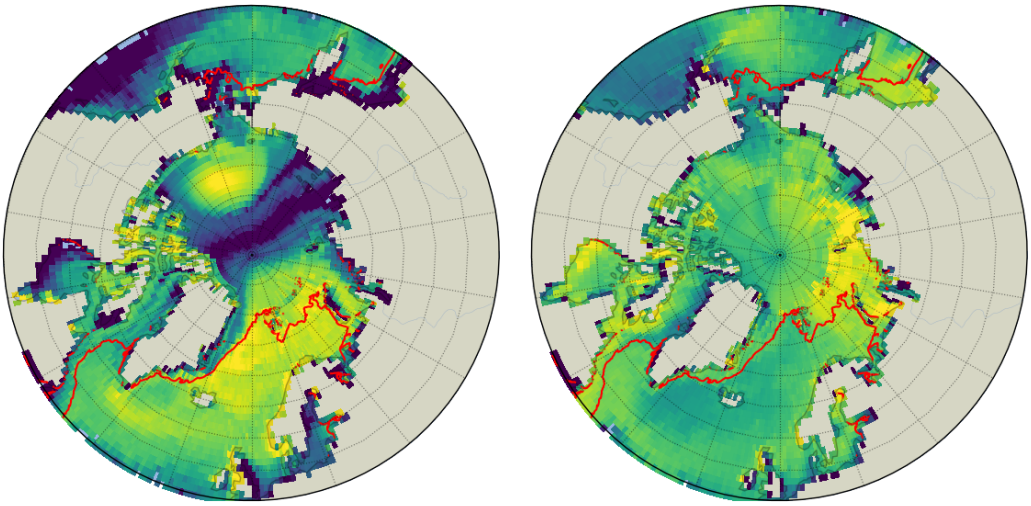

(a) Winter (original) (b) Summer

Figure A.18: Sensitivity to seasons. Other parameters like figure A.17

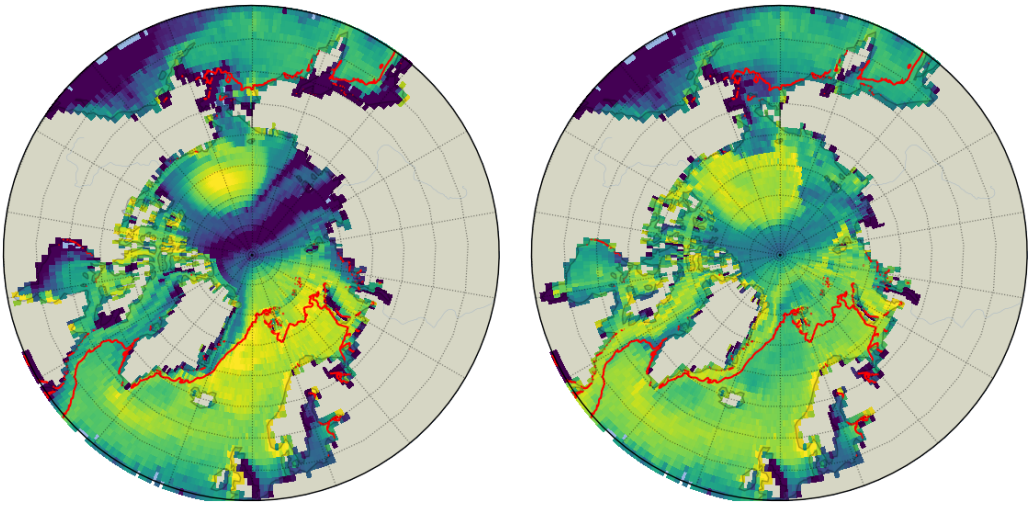

(a) Ice+ocean (original) (b) Only ocean

Figure A.19: Sensitivity to kernel and method of advection. Other parameters like figure A.17

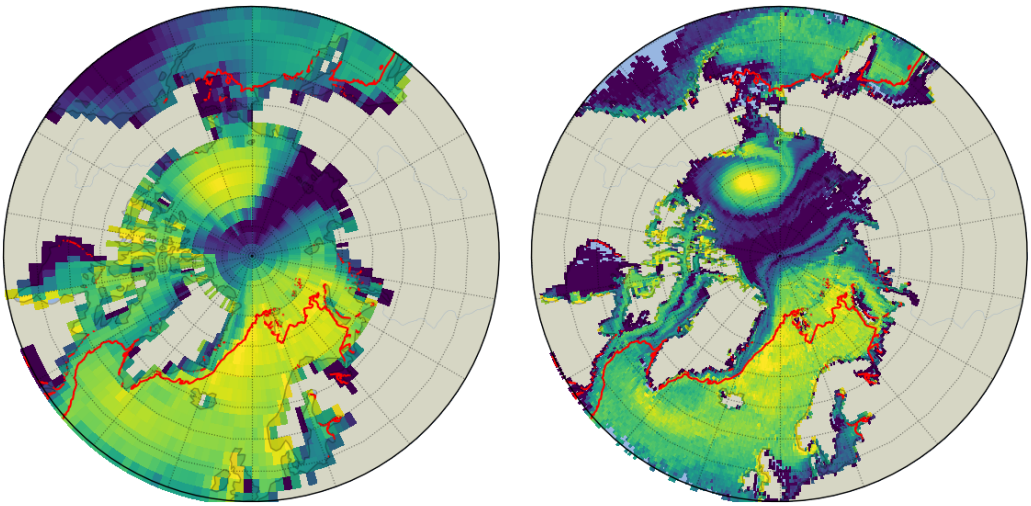

(a) Resolution = 2 degrees (b) Resolution = 0.5 degree

Figure A.20: Sensitivity to resolution. Other parameters like figure A.17

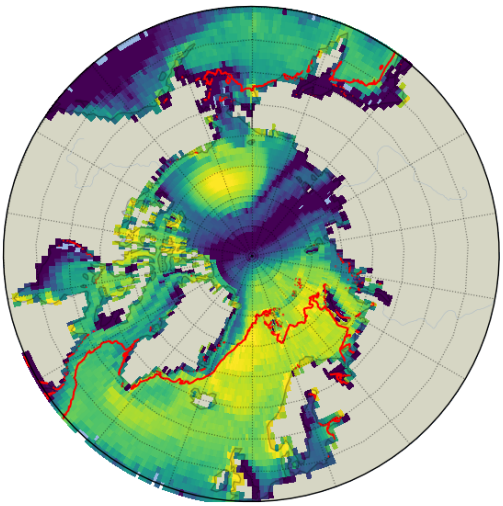

(a) 5 %

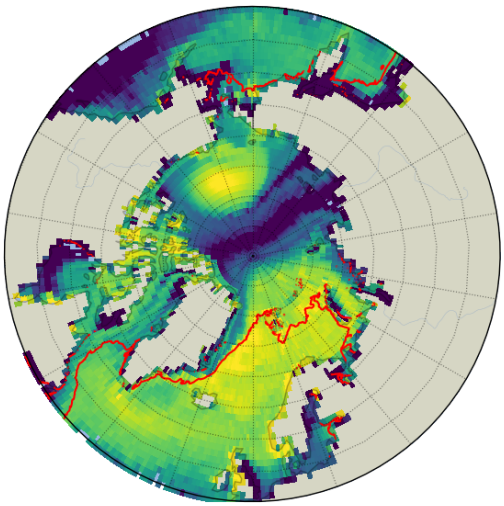

(b) 30%

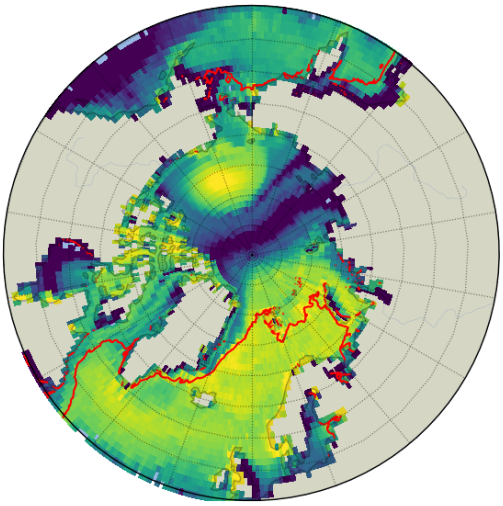

(c) 60 %

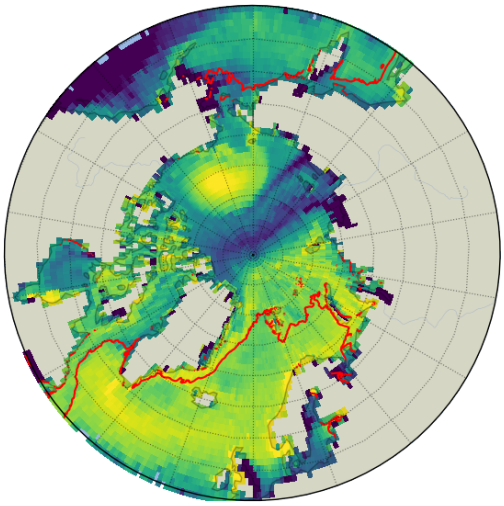

(d) 95%

Figure A.21: Sensitivity to sea ice edge in kernel. Other parameters like figure A.17

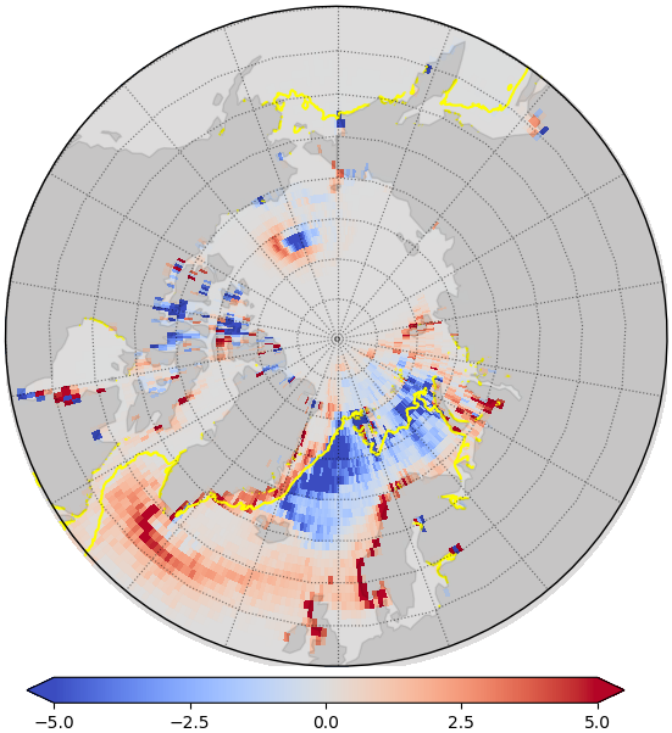

Figure A.22: Difference between extent of 5% (figure A.21a) and 95% (figure A.21d)